



VERTIFLIGHT TECHNOLOGIES IN LEONARDO

Flight Condition Recognition,
Simulation, System Design, Tilt-Rotor
technologies and System Integration

VERTIFLIGHT TECHNOLOGIES IN LEONARDO

Flight Condition Recognition, Simulation, System Design,
Tilt-Rotor technologies and System Integration

PROPRIETARY NOTICE

Contents of the POLARIS Innovation Journal are the personal responsibility of the authors of the individual papers. Authors are entirely responsible for opinions expressed in articles appearing in the Journal, and these opinions are not to be construed as official or reflecting the views of Leonardo or of the listed Committees and Offices. Every article is certified by its corresponding author as being "Company General Use" in compliance with the Security rules and regulations of the Company. The name POLARIS Innovation Journal is property of Leonardo.

All rights reserved. Copyright 2023 Leonardo S.p.A. Reproduction in whole or in part is prohibited, except by permission of the publisher.

contents

03	Editorial
05	Correlation and Accuracy Quantification of Proprotor Loads between Predictions of Comprehensive Aeroelastic Software and Experimental Data
11	Optimizing Automatic Flight Condition Recognition through a Multi-Strategy Machine-Learning Based Approach
18	Developing and Applying Means of Compliance for a Powered Lift Aircraft
26	Automated Robotics for Testing Optimization: an Automatic System for Cockpit Integration Testing
34	Assessment of Numerical Approaches for Modelling Tilt-Rotor Ground Effect stability in Hover and Near Hover Conditions
43	Coupled Torsional Dynamics and Gear Contact Model to Predict Tiltrotor Drive System Loads
51	Editor and Editorial board

VERTIFLIGHT TECHNOLOGIES IN LEONARDO

Flight Condition Recognition, Simulation, System Design,
Tilt-Rotor technologies and System Integration

editorial

Vertical Flight is an expression that has now entered the common language, as we encounter it more and more frequently than in the past. If you have ever wondered what the reasons are, this issue of POLARIS Innovation Journal provides you with comprehensive and interesting answers on this.

Over the last thirty years, Leonardo worked intensely to establish itself as a global leader in Vertical Flight. The evolution and diversification of our products has been mainly driven by the advent of new digital technologies, as well as by greater attention to environmental factors and by the increasingly challenging requirements of users - both civil and military.

To go flying fast between two far locations, or taking off and landing on rather small surfaces while carrying out hovering maneuvers. Until now, performing all these tasks had only been possible by using a helicopter, in its traditional configuration, well known and consolidated in its broad lines.

Today, to carry out those tasks, Leonardo aims at offering a broader spectrum of rotary-wing vehicles featuring significantly different physical configurations, which are identified as Vertical Take Off and Landing (VTOL) aircraft. The VTOL acronym is inclusive of helicopters, but it also identifies a wider family of vehicles that includes tiltrotors such as the AW609, the Rotary Unmanned Air Vehicles (R-UAV) such as the AWHero, as well as the new generation of manned or unmanned rotorcraft that in the foreseeable future will enable flying across large urban areas, thus achieving the so-called Advanced Air Mobility.

Thanks to the implementation of Artificial Intelligence, Autonomous Flight capabilities, Electrification and Cyber Resilience, nowadays we can think of helicopter as of the Smart Helicopter as it has become a highly evolved machine, even by comparing it with machines of the near past.

The convergence of factors that include new design techniques based on the Digital Twin paradigm, use of new materials, new hybrid/electric propulsion concepts, improved aerodynamics and acoustics, is greatly contributing to enhance the sustainability of both the production and the operation of vertical flight aircraft. This, of course, is carried out by always taking into account reliability, performance, costs and comfort for end users.

Leonardo presented these and further innovations at the 79th edition of the Annual Forum & Technology Display of the Vertical Flight Society (VFS), held on May 16th -18th, 2023 in West Palm Beach, FL, USA. There, capabilities of our Company and its calling for technological innovation, were presented and demonstrated.

The VFS Forum is one of the most important world conferences on Vertical Flight, whose comprehensive program covers all the advances in the field of Vertical Flight. It is attended by universities, research centers, OEMs, suppliers and software houses operating in the sector of vertical flight. Over 200 works in different Technical Sessions were discussed during the VFS Forum. Such Technical Papers are specialist documents in which industry experts present the latest theories and breakthroughs across all technology domains of vertical flight. The highlight is the Nikolsky Lectureship award that was established in 1981. It is awarded to an individual who has a highly distinguished career in vertical flight aircraft research and development and is also skilled at communicating his technical knowledge and experience. In 2021 Fabio Nannoni, the temporary technical director of Leonardo's Helicopters Division, was awarded and selected to give such a prestigious lecture.

The VFS Forum also includes Special Sessions in which leaders of "industry, government and academia, gain perspective on the future of vertical flight technology". In such a "Straight Talk from the Top" on a variety of topics, it is possible to receive some insights regarding advanced rotorcraft, Advanced Air Mobility (AAM) and electric VTOL, from leaders of the major rotorcraft manufacturers, managers of military rotorcraft programs and other civil and defense decision makers in government and industry.

VERTIFLIGHT TECHNOLOGIES IN LEONARDO

Flight Condition Recognition, Simulation, System Design,
Tilt-Rotor technologies and System Integration

The Technology Display, which is part of the scenery for the VFS Forum, is the world's leading international exposition on vertical flight technology, where top manufacturers, service providers, defense agencies, universities and research and development organizations showcase their latest innovations about vertical flight technologies such as:

Airframes	Autonomous Aerial Vehicles	Avionics	Components	Display Systems
Electric VTOL	Engine Propulsion	Fuel and Utility Systems (FUS)	Health and Usage Monitoring Systems (HUMS)	Mission Support
VTOL Research and Development	Safety Systems	Simulation and Training	Autonomous VTOL Aircraft	University Research Programs

The VFS international forums give us also the opportunity to take stock of the innovation activities carried out in Leonardo, because the number of competitors who attend our presentations and the interest shown by them, provide us an indirect feedback on the value of the papers presented by our company. At the 2023 edition, Leonardo presented nine papers on the main themes of the VTOL domain.

This POLARIS issue presents six of those themes that go ranging from Machine Learning techniques and analysis of the parameters collected on a production helicopter - for example to reconstruct the type of maneuvers executed - to methodologies for evaluating the correspondence between experimental data and numerical predictions, in this case for the loads generated by the rotor of a tiltrotor.

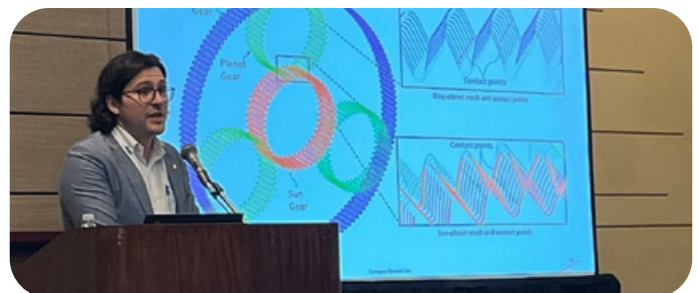
An article concerns the convertiplane (a.k.a. tiltrotor) and the new challenges civil aviation must deal with, both for design and certification of various new functions or devices, such as the “Power Lever” which merges the functions of multiple flight controls into a single inceptor.

Other topics concern the improvement - since the very earliest design stages - of the Human/Machine Interface, where the peculiarities of the convertiplane in terms of mutual interaction between the rotors' wakes and the vehicle close to the ground bring together new complexity, also linked to the specific configuration of those aircraft.

I wish to conclude by reporting with great satisfaction to all the readers that Giuseppe Bucciaglia, one of our authors, was awarded the “Lichten Award runner up” prize during the conference. This prize is reserved for those who, despite having just recently joined our industrial sector, have already started to share their work in international meetings.

Congratulations, therefore, to the many of our young people who today are already designing and implementing the innovations of the future, and enjoy reading!

Head of Aircraft System Design
Luca Medici



Leonardo delegates participating in The Vertical Flight Society's 80th Annual Forum & Technology Display
Left picture: (left to right - top to bottom) Michele Zilletti, Federico Pellegrino, Stefano Mazzetti, Giuseppe Bucciaglia, Enrico Sabatino, Federico Porcaccia, Davide Prederi. Right picture: Nathaniel Albuck



Correlation and Accuracy Quantification of Proprotor Loads between Predictions of Comprehensive Aeroelastic Software and Experimental Data

Giuseppe Bucciaglia, Andrea Duina, Davide Prederi

Leonardo - Helicopters Division

Nowadays, numerical modelling and simulation are essential in the development and certification of new aircraft in order to increase safety and lower costs. Modelling and simulation activities can be divided in three main phases: model building, model correlation and model usage. In this paper, the focus is on model correlation; in particular, for what concerns the estimation of rotor loads using the Leonardo Helicopters in-house comprehensive code, i.e. GyroX. The work presents a summary of an extensive correlation activity performed on the AW609 proprotor and it highlights the modelling key ingredients to consider for accurate load prediction across the conversion corridor. Precisely, the choice of the rotor aerodynamic model, the effects of hub center accelerations and the wing interference are addressed in the correlation process. Furthermore, a metrics is proposed and used to quantify the correlation error between analytical predictions and experimental data coming from flight tests, in order to have a better and immediate comparison between the different model set-ups.

INTRODUCTION

Modelling and simulation are more and more widely used in the development and certification of new aircraft in order to increase safety and reduce costs. The design process of a new aircraft is a challenging task and demands for the interaction of many disciplines, such as flight mechanics, aerodynamics, structural dynamics, loads and aeroelasticity. For what concerns rotor aeromechanics, today the most used simulation tools are comprehensive aeroelastic codes. Generally, these tools exploit a finite element beam formulation for the representation of the structural dynamics of the rotor blade coupled with mid-fidelity numerical methods for the aerodynamic representation, e.g. table look-up methods with corrections for unsteadiness, or even singularity methods based on potential theory.

In this framework, Leonardo Helicopters has its own in-house aeroelastic software, i.e. GyroX, which is meant to condensate all of the previous disciplines, and hence it is aimed to represent a fast and reliable numerical tool for aeroelastic and aeromechanical simulations of complex rotorcraft configurations.

GyroX gathers more than 20 years of experience in rotorcraft simulations and paves the way towards a multi-comprehensive tool for aircraft design and analysis. Modelling and simulation activities can be divided in three main phases: model building, model correlation and model usage. This paper focuses on model correlation, showing a summary of an extensive rotor loads correlation activity between flight tests data of the AW609 proprotor and analytical predictions obtained using the aeroelastic tool GyroX. Many correlation activities on rotor loads were presented in several papers in the past. Valuable and recent examples can be [\[1\]](#) and [\[2\]](#). However, the proposed work features the following main strengths with respect to papers already present in literature. First, it is based on experimental data recorded during the flight campaigns of the AW609 tiltrotor. Another peculiarity of the paper is the focus on modelling elements to include in the simulation in order to obtain the desired accuracy of the prediction all along the conversion corridor. Finally, the paper tries to overcome the arbitrary rating of the level of correlation (resulting in sentences like “well correlated”, “reasonable correlation”, etc.) proposing metrics capable to quantify the correlation error.

VERTIFLIGHT TECHNOLOGIES IN LEONARDO

Flight Condition Recognition, Simulation, System Design,
Tilt-Rotor technologies and System Integration

AW609 PROPROTOR DESCRIPTION

A brief description of the AW609 proprotor is provided in this section.

The 3-bladed proprotor has a diameter of 26.0 feet, the blades have a high non-linear twist and squared tips. The proprotor is stiff in plane with a gimballed hub and flexible yoke. The rpm varies between the VTOL/CONVERSION mode and the AIRPLANE mode. Figure 1 shows an image of the proprotor system.

ANALYTICAL MODEL

Exploiting the capabilities of GyroX software, the rotor structure is represented with beam finite elements and all the rotating components are included in the model, i.e. control chain circuit, hub and blades. Figure 2 shows the AW609 proprotor structural model.

From the aerodynamic point of view, the user can choose among different aerodynamic modelling techniques, such as lifting lines, thin vortex lattices and thick surface panels for solid bodies as depicted in Figure 3.

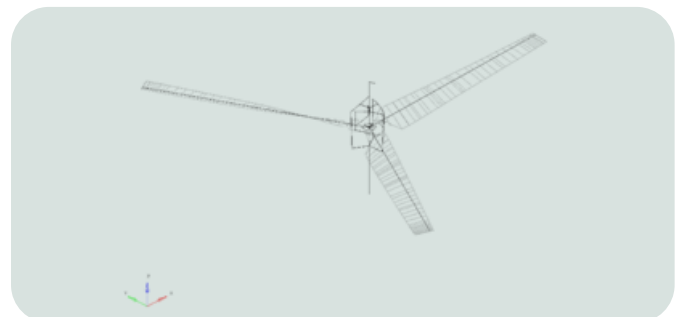
Within this work, the model chosen to represent the rotor aerodynamics is a lifting line with a paneled wake, which can be prescribed as a helicoid or set free to naturally evolve during the simulation.

Procedures of the GyroX solution can be either in the time domain or in the frequency domain (exploiting the harmonic balance method). The latter approach is used in order to obtain the results presented in this paper. In this way, each simulation is a snapshot of a specific time slice of a maneuver. The setup makes use of the above explained rotor model, where the experimental flight data are imposed in terms of:

- environmental conditions
- flight airspeed
- load factor
- aircraft attitude (i.e. angle of attack and sideslip)
- nacelle angle
- rotor rpm
- rotor commands (i.e. collective and cyclic inputs).



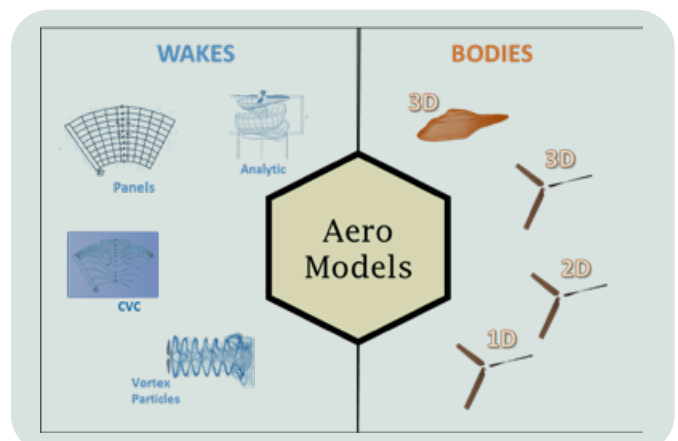
1 – AW609 Proprotor



2 – Structural model of the AW609 proprotor

CEPS THEORY AND DEFINITION

The need for useful metrics to quantify the level of correlation of rotor loads between analytical predictions and data recorded during flight tests has led to the development of an index called CEPS (Correlation Error for Periodic Signal). This index provides the numerical evaluation of the correlation error and gives an immediate feedback among the results obtained with the different models set-ups. In literature, it is possible to find some indices that evaluate the level of correlation between signals. Two examples can be found in [3] and [4]. However, these tools do not take into account some aspects that can be relevant for rotor loads correlation.



3 – Aerodynamic models available in GyroX simulations

Considering steady flight conditions characterized by time-constant rotor commands, aircraft and rotor speed, aerodynamic attitudes and angular rates, the resulting rotor loads are periodic functions of the rotor azimuth. Therefore, it is possible to compare the loads azimuthal-history obtained with the so-called *snapshot* analysis in the frequency domain, with the corresponding experimental flight data in one rotor revolution. Because both the numerical prediction and the experimental data are periodic signals, also the Fourier coefficients can be directly compared in terms of harmonic amplitudes and phases.

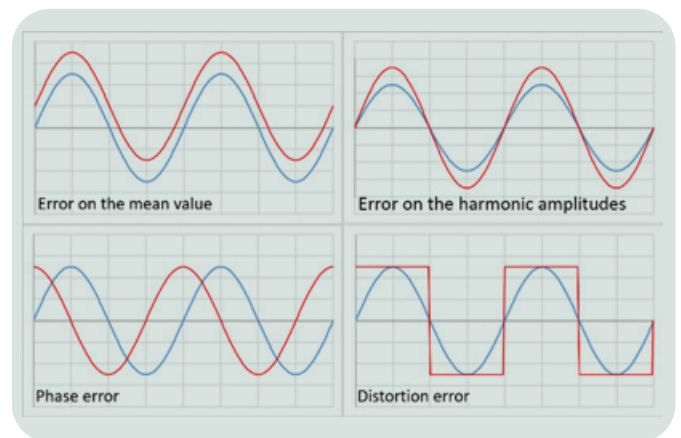
The CEPS is based on the following basic hypothesis:

- Steady flight condition, in order to have periodic signals;
- Already processed measurement error, therefore the experimental signal can be used as a reference to estimate the simulation error;
- Loads time history approximated by using a certain number of harmonics.

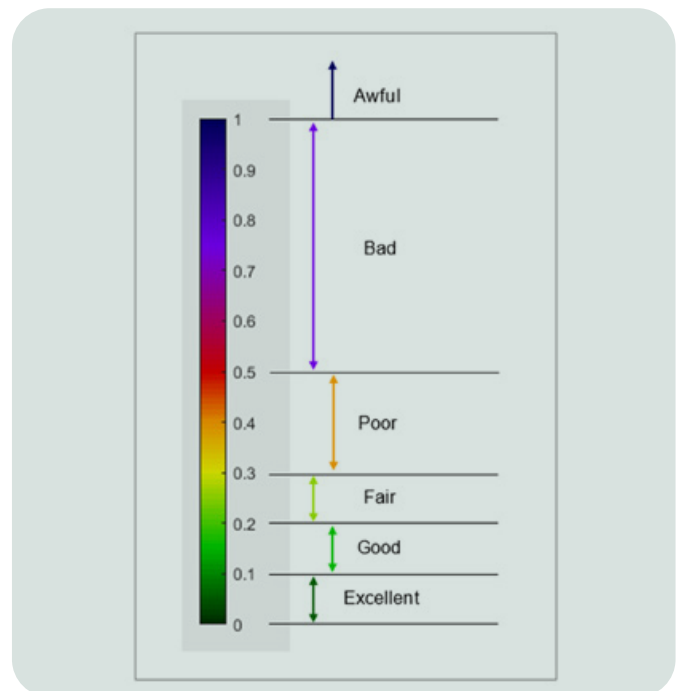
The CEPS is reported in equation (1). It provides a global non-dimensional correlation error made up of four different sub-components: the error on the mean value (ε_0), the error on the harmonic amplitudes (ε_a), the phase error (ε_ψ) and the distortion error (ε_d), that is related to the different wave forms between the two signals. Figure 4 shows an example for each of these four types of error.

$$CEPS = \sqrt{\varepsilon_0^2 + \varepsilon_a^2 + \varepsilon_\psi^2 + \varepsilon_d^2} \quad (1)$$

Based on the application of CEPS in several correlation activities performed on different kinds of rotorcrafts, the following rating scale can be used to evaluate the level of correlation achieved (see Figure 5).



4 - Example of the sub-components of the CEPS



5 - CEPS rating scale

CORRELATION ACTIVITY

Three steady level flights at different nacelle angles (covering the entire conversion corridor) are chosen for the correlation activity. In this way, all the peculiarities of the different flight modes can be analyzed. Table 1 summarizes the selected conditions.

Helicopter mode condition

A fundamental aspect to obtain a properly estimation of rotor loads in helicopter mode condition is related to the selection of the aerodynamic model.

Flight condition ID	Nacelle angle [deg]	EAS [kts]	Pressure Alt. [ft]
1	90 (helicopter mode)	62.0	3714.0
2	50 (conversion mode)	142.0	4311.0
3	0 (airplane mode)	200.0	13279.0

Table 1 - Flight conditions selected for the correlation activity

VERTIFLIGHT TECHNOLOGIES IN LEONARDO

Flight Condition Recognition, Simulation, System Design,
Tilt-Rotor technologies and System Integration

Indeed, as shown by the results that follow, when flight velocity is low, the wake remains close to the rotor plane and its influence must be evaluated more precisely.

Therefore, the usage of lifting line for the body discretization with a free panel wake (LLFW - Lifting Line Free Wake) increases the accuracy of the analytical prediction with respect to a lifting line with a prescribed panel wake (LLPW - Lifting Line Prescribed Wake) model.

Figure 6 shows the azimuthal history between the experimental data and the analytical predictions of the blade beam bending at 20% of the rotor radius, whereas the CEPS values and its sub-components are reported in Table 2.

From these data, it can be inferred that the LLFW leads to a better beam bending correlation, with CEPS reduction of about 30% w.r.t. the LLPW. In accordance with the CEPS rating scale reported in Figure 5, using LLFW the beam bending correlation can be rated between good and fair, whereas using LLPW the correlation can be graded between fair and poor. Looking at the sub-components of the CEPS, it is possible to observe that the LLFW model allows to reduce the error on the harmonic amplitudes, the phase error and the distortion error. On the contrary, the error on the mean value is not affected by the aerodynamic model.

error	LLFW	LLPW
ε_0	-0.001	0.001
ε_a	-0.136	-0.200
ε_ψ	-0.085	-0.125
ε_d	0.136	0.182
CEPS	0.210	0.298

Table 2 – CEPS values for blade beam bending moment at station 20%R – flight condition 1

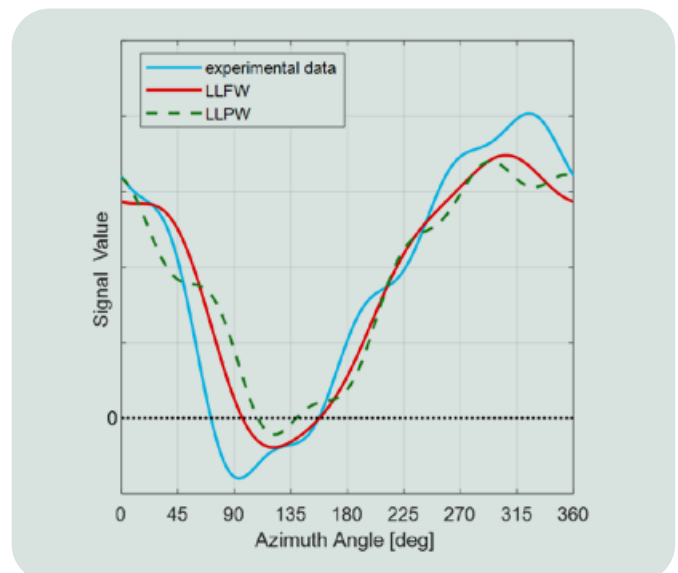
Conversion mode condition

The performed correlation activity allows confirming the need to take into account hub center accelerations in order to properly estimate rotor loads. Taking advantage of the GyroX capabilities, in this snapshot simulation, the rotor is shaken in its plane and out of it, with the accelerations recorded during this flight condition.

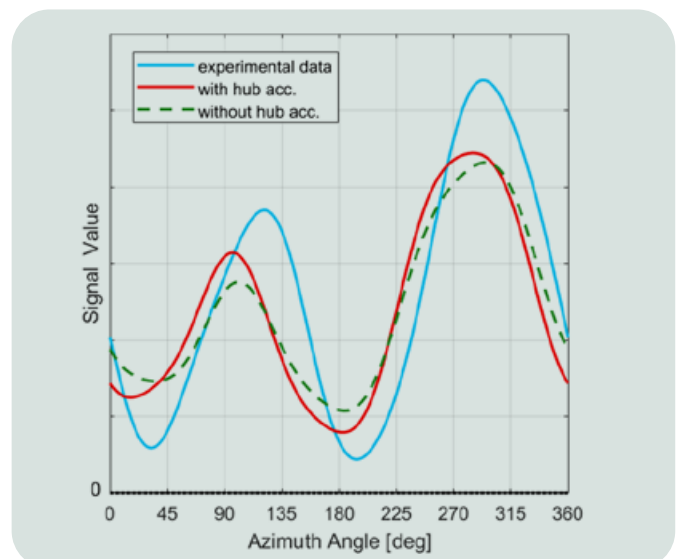
Of course, using hub center accelerations recorded in flight, the simulation is not completely predictive. Therefore, in the future it could be useful to develop a pylon model in order to predict also hub center accelerations. The results below show the comparison of the experimental data with the analytical prediction obtained by applying or not the hub center accelerations.

Figure 7 shows the azimuthal history between the experimental data and the analytical predictions of the blade chord bending at 20% of rotor radius, whereas CEPS values and its sub-components are reported in Table 3.

It is possible to observe that the introduction of hub center accelerations leads to a better chord bending correlation, with CEPS reduction of about 20%. Referring to the CEPS rating scale reported in Figure 5, the correlation is fair, both considering or not the hub center accelerations.



6 – Azimuthal history of blade beam bending moment at 20%R – flight condition 1



7 – Azimuthal history of blade chord bending moment at 20%R – flight condition 2

When not applying hub center accelerations the rating is close to the poor region, but with the introduction of hub accelerations the rating moves towards the good region. Looking at the sub-components of the CEPS, the introduction of hub center accelerations reduces the harmonic amplitude error and the distortion error. On the contrary, the phase error gets slightly worse, whereas the error on the mean value is unaffected by the introduction of the hub center accelerations.

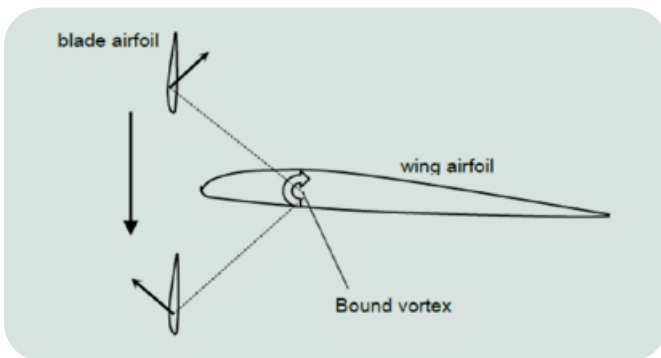
error	with hub acc.	Without hub acc.
ε_0	-0.051	-0.047
ε_a	-0.156	-0.217
ε_ψ	0.100	0.059
ε_d	0.108	0.160
CEPS	0.221	0.280

Table 3 – CEPS values for blade chord bending moment at station 20%R – flight condition 2

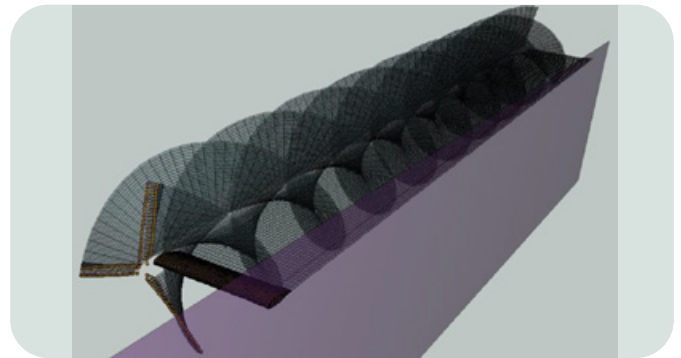
Airplane mode condition

The analyses performed show that in airplane mode conditions the rotor-wing interference cannot be neglected because it is the fundamental source of two basic physical phenomena.

The first one is related to the lift of the wing and the second one is related to the thickness of the wing. The effect of a lifting-only wing is sketched in Figure 8.

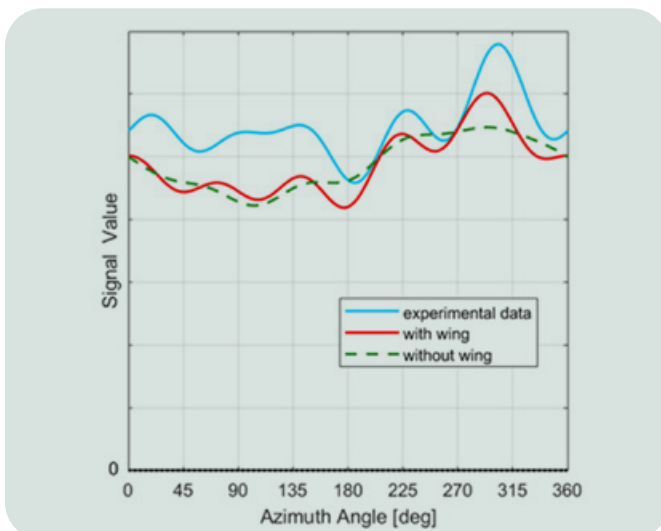


8 – Rotor-wing aerodynamic interference



9 – Isolated rotor + 3D wing + symmetry plane

The blade airfoil is rotating ahead of the leading edge of the wing and so it undergoes the inductive effect of the wing itself, which is producing a large amount of lift and so it features large inductive power. Indeed, the blade experiences a *down-wash* which decreases the angle of attack of its airfoils as it passes close to the suction side of the wing, whereas the blade experiences an *up-wash* with consequent increase of the angle of attack as it passes close to the pressure side of the wing.



10 – Azimuthal history of blade chord bending moment at 20%R – flight condition 3

The second contribution is related to the thickness of the wing and it is a sort of blockage effect.

In the following, the correlation results obtained by considering the 3D aerodynamic model of the wing combined with the symmetry plane (in order to recover the influence of the other half wing and rotor) are compared with the results of the isolated rotor simulation and the experimental flight data.

Figure 9 shows the set-up of the analysis with 3D wing and symmetry plane. Figure 10 shows the azimuthal histories of the experimental data and the analytical predictions of the blade chord bending at 20% of rotor radius, whereas CEPS values and its sub-components are reported in Table 4.

The introduction of the wing reduces the error on harmonic amplitudes and the distortion error, whereas the error on the mean value and the phase error are approximately unchanged. The resulting reduction of the CEPS is around 15%.

VERTIFLIGHT TECHNOLOGIES IN LEONARDO

Flight Condition Recognition, Simulation, System Design,
Tilt-Rotor technologies and System Integration

error	with wing	without wing
ε_o	-0.107	-0.108
ε_a	0.003	-0.017
ε_ψ	0.011	0.013
ε_d	0.061	0.101
CEPS	0.124	0.150

Table 4 – CEPS values for blade chord bending moment
at station 20%R – flight condition 3

CONCLUSIONS

The present work is a summary of an extensive correlation activity performed on the proprotor of the AW609. The focus is on the most important ingredients for rotor loads predictions that need to be included in the simulations. Furthermore, a metrics called CEPS is here proposed, to evaluate the accuracy of the analytical predictions w.r.t. the data measured during experimental flights and to quantify the improvements

in the correlation due to the investigated modelling elements. The main conclusions on the rotor loads correlation task are highlighted below:


1. A lifting line with a free wake panel model should be preferred to a prescribed paneled wake for flight conditions at low advance ratio, in order to better catch the aerodynamics interactions between wakes and bodies.
2. The simulations confirm that the introduction of hub center accelerations impacts the accurate estimation of rotor loads.
3. The performed analyses show that in airplane mode the rotor-wing interference effects are a relevant source of oscillatory loads.
4. The CEPS metrics shows the capability to quantify the correlation error. Moreover, it also allows to identify the weight of each sub-component (error on the mean value, error on the harmonic amplitudes, phase error and distortion error) contributing to the global error.
5. The CEPS metrics is essential to identify the improvements of the correlation when the differences are limited or when the inference from results, such as the azimuthal history, may be misleading.

Giuseppe Bucciaglia: giuseppe.bucciaglia@leonardo.com

REFERENCES

- [1] Kottapalli, S., and Acree, C.W., “Correlation of Full-Scale Isolated Proprotor Performance and Loads”, Proceedings of the 75th Annual Forum and Technology Display the Vertical Flight Society, Philadelphia, Pennsylvania USA, May 2019.
- [2] Berend, G., van der Wall, B.G., Lim, J.W., Smith, M.J., Jung, S.N., Bailly, J., Baeder, J.D., and Boyd, D.D., “The HART II international workshop: an assessment of the state-of-the-art in comprehensive code prediction”, CEAS Aeronautical Journal, (4), 2013, pp. 223–252. doi: 10.1007/s13272-013-0077-9.
- [3] Nabuco, B., Friis, T., Tarpo, M., Amador, S., Kastanos, E.I., and Brincker, R., “Nonlinear Strain Estimation Based On Linear Parameters”, Proceedings of the ASME 2018 37th International Conference on Ocean, Offshore and Arctic Engineering, Madrid, June 2018.
- [4] Smith, M.J., Jacobson, K.E., and Afman, J.P., “Towards Certification of Computational Fluid Dynamics as Experiments for Rotorcraft Applications”, The Aeronautical Journal, Vol. 122, (1247), Jan. 2018, pp. 104–130. DOI: 10.1017/aer.2017.118.

Proprietary information of Leonardo S.p.A. – General Use. All rights reserved. Neither the articles nor Company information shall be published, reproduced, copied, disclosed or used for any purpose, without the written permission of Leonardo S.p.A.



Optimizing Automatic Flight Condition Recognition through a Multi-Strategy Machine-Learning Based Approach

Eugenia Villa¹, Francesco Zinnari¹, Giovanni Coral¹, Gabriele Cazzulani¹, Mara Tanelli¹, Andrea Baldi², Ugo Mariani², Daniele Mezzanzanica²

¹Politecnico di Milano, ²Leonardo – Helicopters Division

The Flight Condition Recognition (FCR) plays a fundamental role in monitoring the usage of helicopters, as the usage spectrum determines the lifecycle and replacement of its components. Automated FCR capabilities are realized through algorithms that enable to detect the aircraft manoeuvres by appropriately processing the on-board sensors measurements. This allows monitoring the actual usage thanks to the reconstruction of the real usage spectrum, which enables customizing maintenance operations and condition-based maintenance strategies. However, designing an effective automatic FCR system is a challenging task, due to the complex machine dynamics that characterize the different flight regimes. In this work, we show how to optimize a machine-learning based approach to the FCR design by exploiting a multi-strategy time-series segmentation framework, which combines two supervised learning approaches that leverage sliding windows and stacking ensembles to produce reliable estimates of the flown regimes. This approach is validated on a large experimental dataset of nearly 500 labelled flights from two helicopter models, demonstrating the effectiveness of the proposed strategy in predicting the different manoeuvre types, and its improvement over a single-strategy approach.

INTRODUCTION AND MOTIVATION

The definition of the real usage spectrum of a helicopter is a fundamental task to understand the fatigue loading conditions that a helicopter has been subjected to during its lifetime. The Flight Condition Recognition (FCR) provides indeed a reliable indicator of the real usage of helicopters, supporting the definition of improved maintenance plans, with replacement times and inspection intervals tailored to helicopters actual usage, thus enabling condition-based maintenance schedule [1][2][3]. The latter overcomes the limitations of a time-based maintenance plan defined at design time, based on an ideal usage spectrum that does not always match the actual one. In this way, by avoiding untimely maintenance interventions, clear advantages in terms of both safety and cost reduction can be reached [4]. For these reasons, the development of efficient and accurate regime recognition algorithms has always been a high-priority and challenging task [5]. Multiple approaches have been indeed proposed over time to

classify the manoeuvres performed by an aircraft by appropriate processing of on-board sensors measurements. Until the recent past, the most common approach for FCR was to use deterministic models relying on rules and thresholds established by domain experts based on *a-priori* known physical models [6][7]. However, those approaches show some clear limitations. First of all, they require a manual and time-demanding continuous refinement of the employed rules and thresholds that end up being highly dependent on the helicopter model, which affects the generalization capabilities. Moreover, those kinds of algorithms work on one dimension (i.e. one signal) at a time, therefore they often feature some grey areas where the employed rules overlap, so that regimes cannot be always properly distinguished. Finally, those algorithms are typically not scalable with the number of signals recorded by on-board sensors. To overcome such limitations, Machine Learning (ML)

VERTIFLIGHT TECHNOLOGIES IN LEONARDO

Flight Condition Recognition, Simulation, System Design,
Tilt-Rotor technologies and System Integration

techniques have been recently proposed to automatize the FCR task. This approach features the main advantage of being automated, easily adaptable to different aircraft configurations, and scalable along with the number of available measurements. However, the works in which the ML approaches are applied to FCR, are still few and limited. The most part of them employ supervised algorithms such as Neural Networks or Decision Tree Classifiers, to recognize a restricted set of regimes that do not include the whole usage spectrum of the aircraft [4][8]. Thus, their results cannot be considered reliable enough. Similarly, [9] shows how to use a Markovian approach to recognize a wider set of flight conditions, but it has been tested only on a limited set of simulated flight data, which makes the results again not completely reliable.

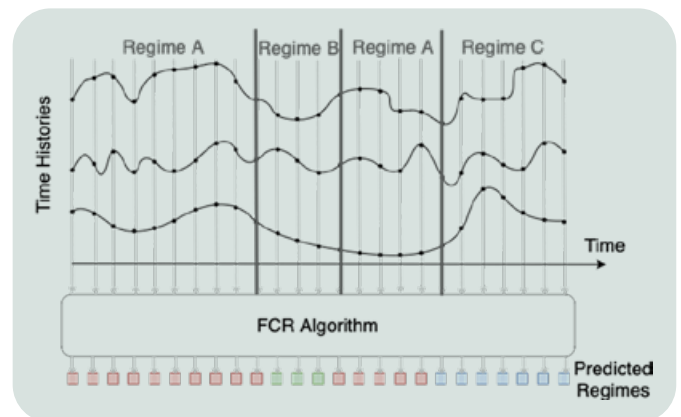
Finally, in [10] the FCR task is solved in a single-strategy time-series segmentation framework based on stacking ensemble learning on multiple sliding windows. The proposed algorithm is validated on a large experimental dataset with 53 flight regimes, showing accuracy of 97%.

In this work, we show how the ML-based approach proposed in [10] can be optimized by exploiting a multi-strategy time-series segmentation framework. The proposed methodology, therefore, combines two supervised learning approaches that leverage sliding windows and stacking ensembles to produce reliable estimates of the flow regimes. The second additional strategy is introduced to increase the robustness to the variability in manoeuvre duration. The approach is validated on a large experimental dataset of nearly 500 labelled flights from two helicopter models, demonstrating the effectiveness of the proposed strategy in predicting the different manoeuvre types, and its improvement over a single-strategy approach. (see Video in [11])

PROBLEM SETTING AND DATASET DESCRIPTION

The final objective of this work is to optimize the time-series segmentation algorithm proposed in [10], to design an automatic and efficient methodology to reconstruct the usage spectrum of a helicopter during its entire flights. The algorithm takes as input the time-series recorded by on-board HUMS sensors during real flights and provides as output the regime performed by the aircraft at each time-step.

As shown in Figure 1, two main challenges arise: first of all, in complete flights, regimes are seamlessly performed, thus the start and end points of each regime are *a-priori* unknown. Besides, different regimes (as well as different instances of the same regime) can be characterized by significantly different duration in time, so that the algorithm must efficiently manage the recognition of regimes with different duration.



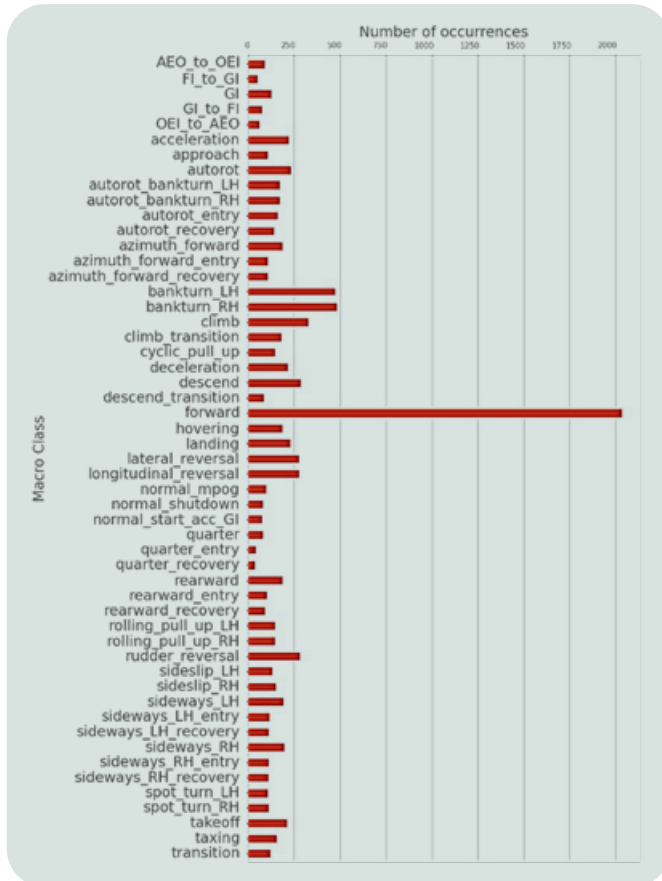
1 – The FCR algorithm applied on an entire real flight.
The start and end points of each regime are *a-priori* unknown
and their duration is variable

To this end, we propose a multi-strategy supervised approach that exploits a large set of labelled Load Survey Flights. This enables to learn performed regimes based on available HUMS signals that use a sliding window approach to automatically segment the flight time-series, namely to identify starting point and duration of each regime from full flight data. The algorithm has been developed by exploiting a large experimental dataset of nearly 500 labelled flights from two helicopter models collected during Load Survey operations. The set of measurements obtained from the on-board sensors is the same for both the helicopters.

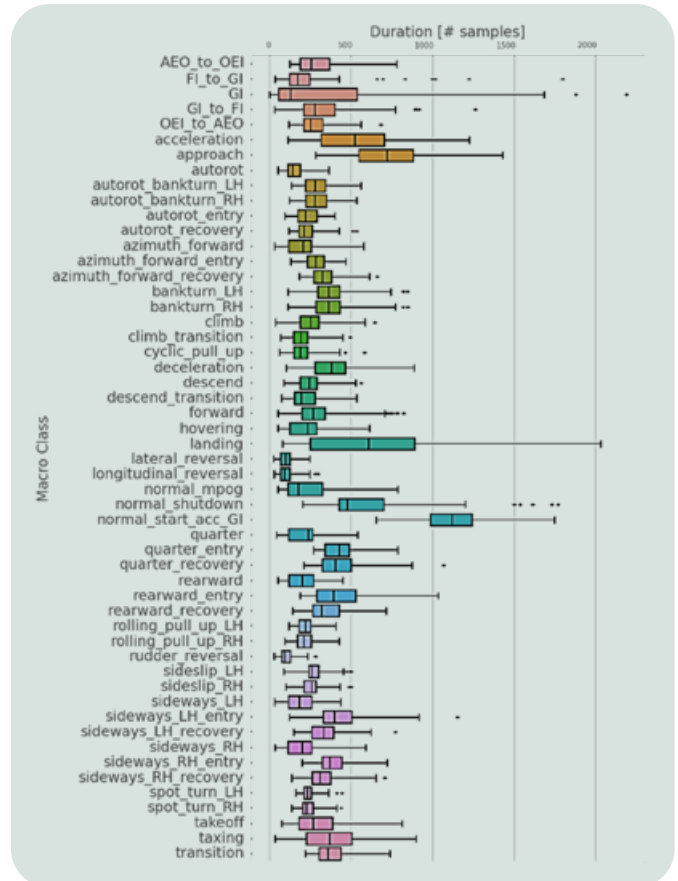
Besides parameters for flight identification, it includes 4 pilot commands, 3 signals for each aircraft engine, 2 measured ground speeds, 6 attributes related to flight dynamics angles, 6 attributes representing speeds and accelerations, 4 attributes describing environmental conditions.

Figure 2 shows the number of manoeuvres available for each macro-class in the design set. These aggregations have been defined with the support of domain experts, so that once the algorithm correctly recognizes the macro-classes, it is easy to further reconstruct specific spectrum conditions by exploiting simple deterministic models applied to relevant signals. In this way, we enable a one-to-one correspondence with the fatigue spectrum. After an accurate exploratory data analysis and data cleaning stage, a peculiarity characterizing our dataset has emerged, as shown in Figure 3. Manoeuvres feature indeed high variability in time duration, between classes as well as within the same class.

As we already mentioned, particular attention should be posed to this aspect since it can strongly affect the algorithm's capability of recognizing manoeuvres over an entire free flight. The optimized methodology proposed in this work specifically aims at improving the capability of the ML-based algorithm to efficiently deal with manoeuvres of different duration.



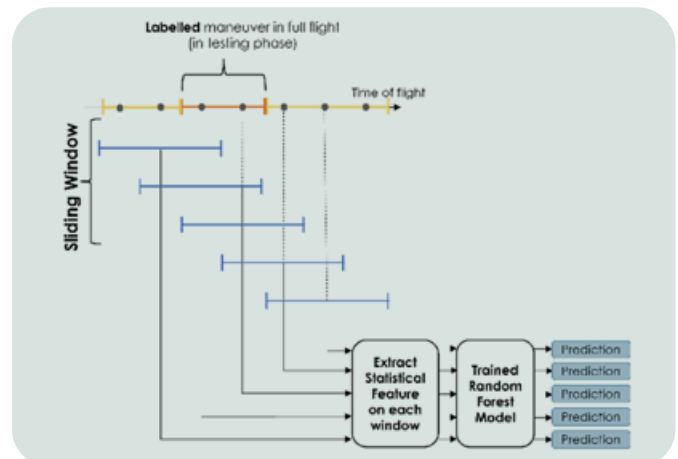
2-Number of instances in the whole dataset for each of the 53 macro-classes considered



3-Distribution of manoeuvres' duration for the considered 53 macro-classes

THE SINGLE-STRATEGY APPROACH: AN OVERVIEW

Relying on the same dataset described in the previous section, in [10] the authors propose a ML-based single-strategy approach for the FCR task. Since we want to show how this approach can be improved by integrating it within a multi-strategy framework, it is essential to provide a brief description of its key aspects. After a smart split of the data into stratified flights train and test sets, the single-strategy approach trains a Random Forest (RF) classifier on a relevant set of statistical features extracted from each manoeuvre instance belonging to the training set. The considered features are statistical descriptors of the input time series, such as mean, standard deviation, maximum and minimum. They are computed for both the available signals and their time derivatives, thus providing a comprehensive description of the aircraft dynamics over the considered time-interval.



4-Sliding window approach

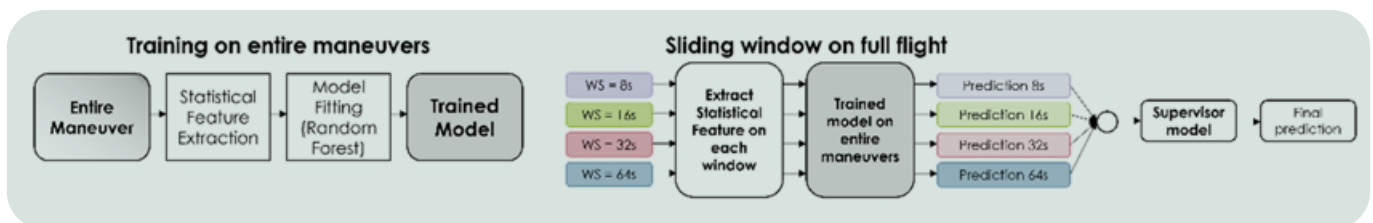
VERTIFLIGHT TECHNOLOGIES IN LEONARDO

Flight Condition Recognition, Simulation, System Design,
Tilt-Rotor technologies and System Integration

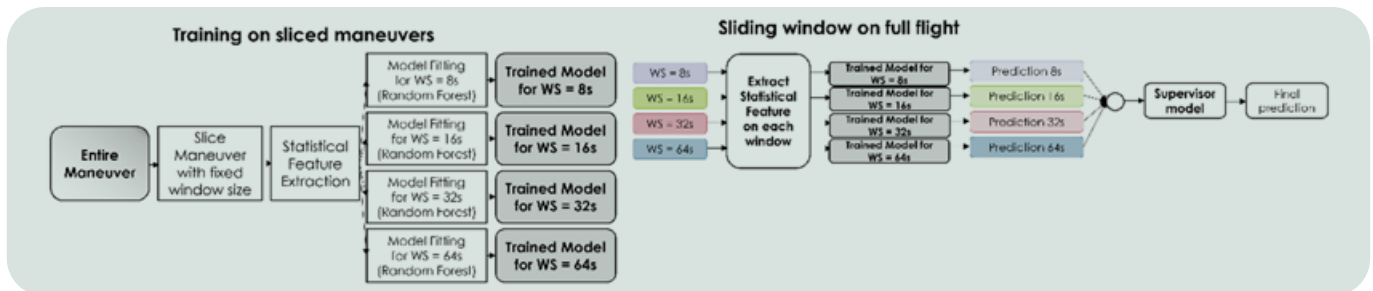
Hence, given the start and end point of the instance and the correspondent extracted statistical features, the obtained RF model is initially able to recognize the performed manoeuver.

However, since in a real full flight the start and end points of each instance are not known, a sliding-window approach is adopted. Specifically, a window of fixed size slides over the record of the entire flight, the correspondent statistical features are extracted from the windowed time series, and, by applying the previously trained RF model to each window, the predicted manoeuver prediction is obtained. Figure 4 summarizes the key aspects of such a sliding-window approach.

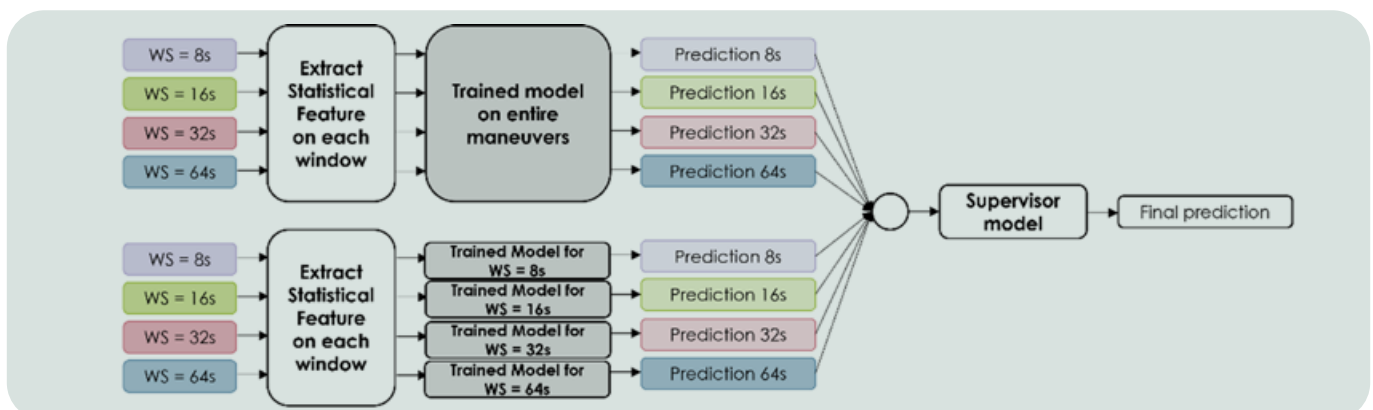
In order to enable the recognition of manoeuvres of different duration, 4 different window sizes are employed, specifically of 8, 16, 32, 64 seconds. Predictions obtained in the four scenarios are then aggregated through a second level supervisor. The structure of the overall single-strategy pipeline is shown in Figure 5. Despite its good overall performance, a drawback of this approach is that the RF model is actually trained on statistical features extracted from the full manoeuvres that may present different time-duration, while it is applied on full flights by partitioning the data over the aforementioned 4 time-windows, which are used to extract the features based on which the model takes its decisions. Thus, it may happen that features and models may be mismatched. The idea of devising an additional strategy, thus, aims to overcome this problem by optimally learning regimes of different duration by constructing different models over the 4 time-windows (see Figure 6).



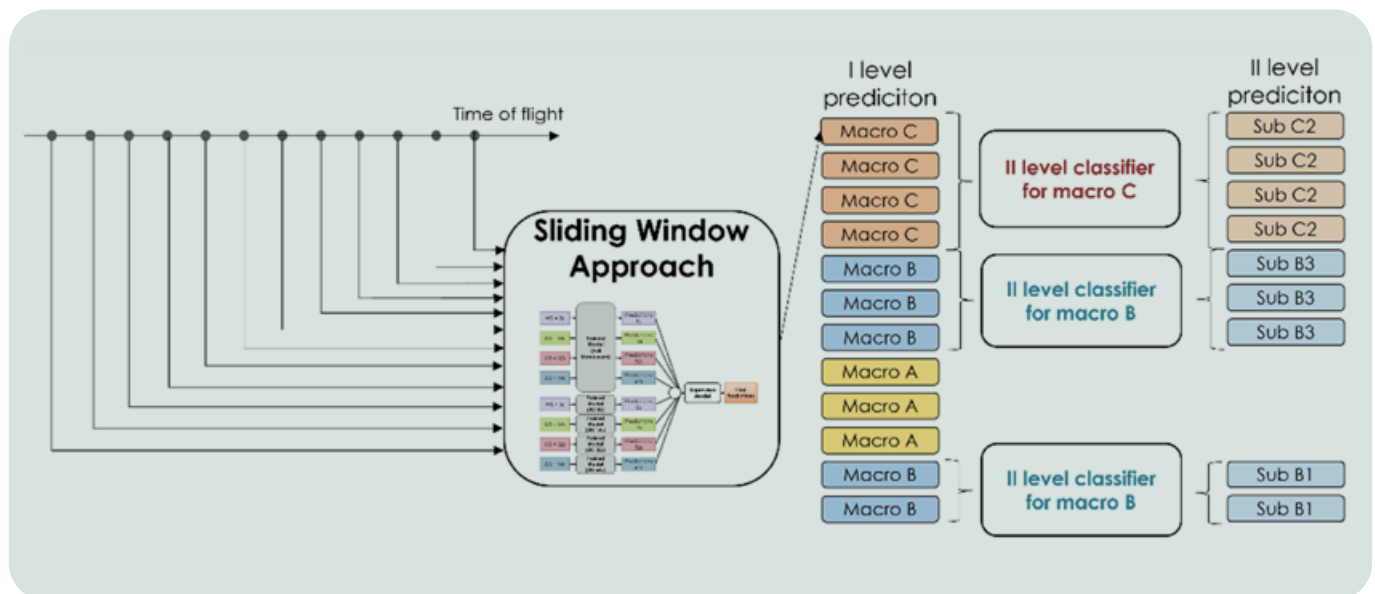
5–Key steps of strategy 1: a ML-based model is trained on statistical features extracted from entire manoeuvres and then applied on feature extracted from 4 sliding windows of different size to obtain 4 correspondent predictions. The final prediction is obtained from the previous through a supervisor model



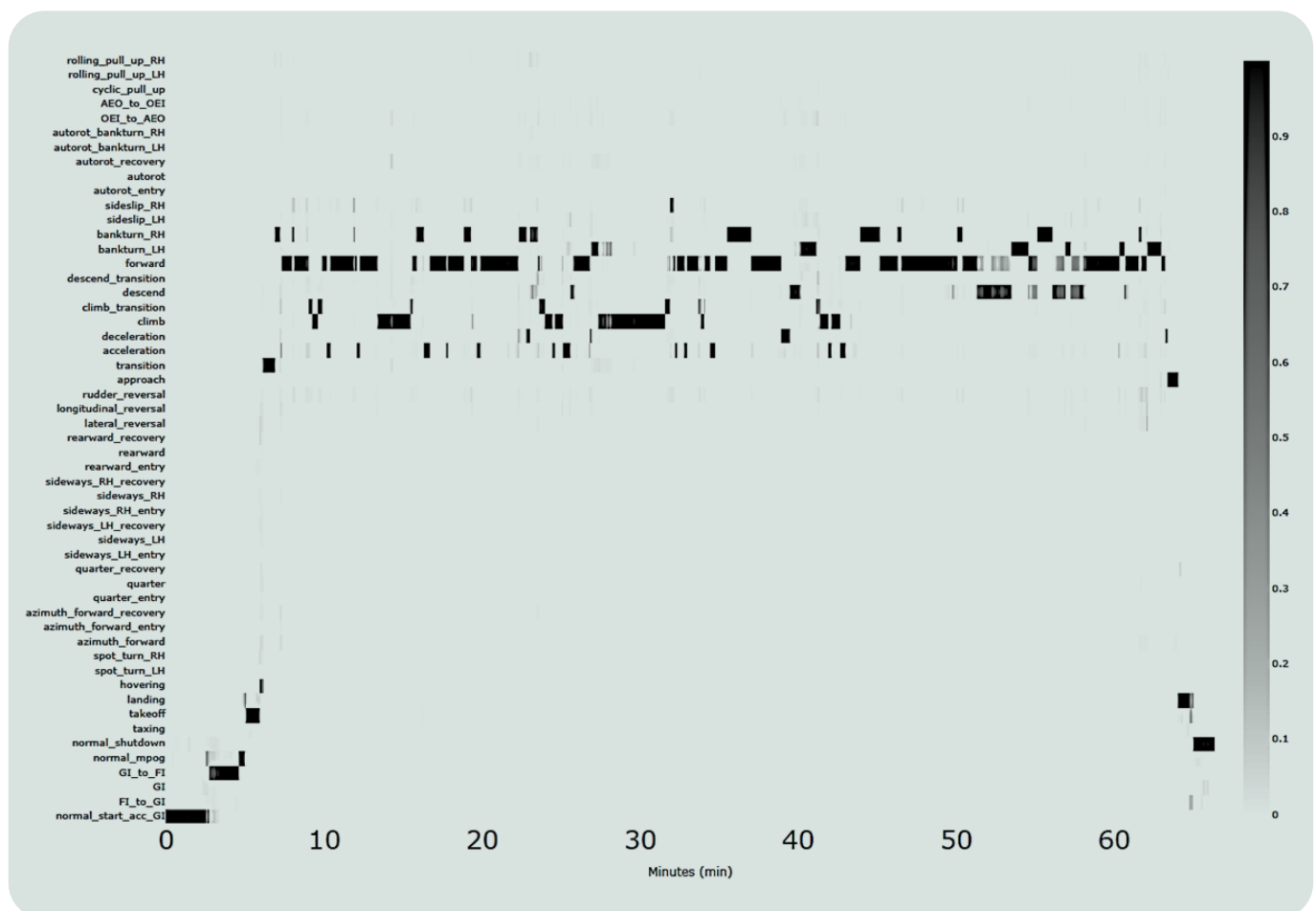
6–Key steps of strategy 2: 4 ML-based models are trained on statistical features extracted from sliced manoeuvres with window size of 8, 16, 32, 64 s and then applied on feature extracted from 4 sliding windows of correspondent size to obtain 4 predictions. The final prediction is obtained from the previous through a supervisor model



7–The optimized multi-strategy approach exploits both strategies to obtain through a final supervisor the final predictions



8 – The 53 macro-classes recognized by the first level classifier of the multi-strategy approach are then split into sub-categories through simple rule-based models (second level classifier) in order to obtain a one-to-one correspondence with the usage spectrum



9 – Heatmap of predicted probability distributions over time. Darker markers denote higher probability that a given regime was executed during the considered time interval

OPTIMIZED MULTI-STRATEGY FCR ALGORITHM

The multi-strategy ML-based approach combines the approach in [10] with an additional learning strategy that constructs different models over windowed data, and then uses these dedicated models on the features extracted by each time window on full flights.

To do so, 4 different RF models are trained on manoeuvres appropriately sliced into the 4 fixed size windows. The size of these windows obviously matches the size of the windows employed to slice the full flight. Thus, we obtain 4 distinct RF models, trained on windows of size 8s, 16s, 32s, 64s, that are applied to the feature extracted from sliding windows of the correspondent size. The 4 predictions obtained by these first-level classifiers are then aggregated through a second level classifier consisting of a multivariate logistic regression on the probability distribution over the 53 macro-classes. The overall pipeline of the second strategy is shown in Figure 6.

In order to maximize the performance of the overall FCR algorithm, we decided to exploit both the strategies, aggregating their outputs through a final supervisor that allows us to obtain the final predictions, as shown in Figure 7.

Finally, to have a one-to-one match with the usage spectrum, we introduce multiple deterministic models that, based on the predicted macro-class, can create correspondent sub-categories matching the regimes that belong to the spectrum.

Being simple uni-variate models, they do not require any manual tuning and do not lead to overlapping classes as in the entirely rule-based approaches previously proposed in the literature. Figure 8 shows the complete pipeline of the optimized multi-strategy FCR algorithm.

RESULTS AND DISCUSSION

We now present the results obtained with the optimized multi-strategy FCR algorithm, highlighting in particular the role of the second strategy in improving the final predictions. Due to the unbalance in the different regimes representation in the data, we evaluate the performance by employing macro-averaged metrics such as accuracy, precision, recall and F1-Score.

By computing the metrics independently of each class and then taking their average, the macro-averaged indicators treat each class equally, overcoming the class unbalance. Table 1 shows the results obtained with: strategy-1, strategy-2 and with the multi-strategy approach on 150 test flights. The results demonstrate that strategy-2 singularly recognizes the considered macro-categories with higher F1-score compared to strategy-1. This is due to the enhanced capability to deal with different manoeuvres duration and to recognize relevant trends in the sliding windows, by exploiting models trained on features vectors extracted from the same window sizes. The combination of the two strategies in the multi-strategy approach leads to increase in performances with respect to both the strategies if considered separately. For this reason, we decided to exploit both of them, to reach final accuracy of over 97% and F1-score of 97% in the first classification level.

In addition to the final predictions obtained from the supervisor at each time step, the optimized FCR algorithm also provides the output shown in Figure 9. Here, the heatmap of predicted probability over each macro-class in time is reported: darker markers indicate a higher probability that in the considered time interval a specific regime has been executed. This type of output is particularly useful to complement final predictions as it allows domain experts to understand the confidence level of such predictions and to eventually identify unclear classifications which may correspond to mixed regimes. The latter is also supported by the additional classification layer introduced in the multi-strategy scheme. Indeed, it enables a one-to-one correspondence of the obtained output and the real usage spectrum, while reducing the number of classes considered in the first classification level, hence reducing the risk of over-fitting.

Strategy		Acc.	Prec.	Rec.	F1
Strategy 1	WS=8s	0.72	0.81	0.64	0.63
	WS=16s	0.83	0.85	0.78	0.78
	WS=32s	0.87	0.85	0.83	0.83
	WS=64s	0.73	0.72	0.65	0.63
	Supervisor	96%	94%	95%	94%
Strategy 2	WS=8s	0.89	0.89	0.86	0.88
	WS=16s	0.91	0.91	0.89	0.90
	WS=32s	0.85	0.87	0.83	0.85
	WS=64s	0.72	0.72	0.62	0.70
	Supervisor	96%	96%	95%	96%
Multi-strategy (1+2)	Supervisor	97%	97%	96%	97%

Table 1–Performance metrics with different strategies

CONCLUDING REMARKS

This paper demonstrates the effectiveness of a multi-strategy ML-based approach in solving the FCR problem. The proposed algorithm aggregates - through a final supervisor - two main strategies: the first is trained on entire manoeuvres and embeds the statistical features characterizing the considered macro-class, while the second, trained on sliced manoeuvres, embeds the statistical features characterizing the slice of the considered size. Hence, both contribute to the correct recognition of flight regimes. Specifically, the second strategy introduced in this work improves the recognition of regimes with variable duration.

The multi-strategy approach is able to correctly classify the considered macro-classes with F1-score of 97.05%, improved with respect to both the single strategies.

Besides, given the massive amount of real-life data

employed to test the proposed methodology, the presented results prove the robustness of the multi-strategy approach for FCR.

Furthermore, the proposed approach is flexible and scalable. It enables the recognition of real usage spectra for multiple helicopter models, as far as data are available for training.

It can be easily re-trained if more or different measurements are available from on-board signals. Finally, this efficient way to solve the challenging FCR task by providing actual and reliable usage monitoring of the helicopter components, enables the definition of customized maintenance plans, tailored to the helicopters actual usage, thus the transition to a condition-based maintenance schedule, allowing safety improvements as well as cost reductions.

Andrea Baldi: andrea.baldi01@leonardo.com

REFERENCES

- [1] D. Le and E. Cuevas, "United states federal aviation administration health and usage monitoring system r&d strategic plan and initiatives," in Proceedings of the 5th DSTO International Conference on Health and Usage Monitoring, 2007.
- [2] L.C.J. Milsom, "A study of usage variability and failure probability in a military helicopter," in Third International Conference on Health and Usage Monitoring-HUMS2003, p. 81, Citeseer, 2002.
- [3] J. Jylh'a, M. Ruotsalainen, T. Salonen, H. Janhunen, I. Ven'al'ainen, A. Siljander, and A. Visa, "Link between flight maneuvers and fatigue," in ICAF 2011 Structural Integrity: Influence of Efficiency and Green Imperatives, pp. 453–463, Springer, 2011.
- [4] J. Berry, R. Vaughan, J. Keller, J. Jacobs, P. Grabill, and T. Johnson, "Automatic regime recognition using neural networks," in Proceedings of American Helicopter Society 60th Annual Forum, pp. 9–11, 2006.
- [5] D. Lombardo and K. Fraser, "Importance of reliability assessment to helicopter structural component fatigue life prediction," tech. rep., DEFENCE SCIENCE AND TECHNOLOGY ORGANISATION VICTORIA (AUSTRALIA 2002).
- [6] B. Gene, S. Sarkar, and C. Miller, "Maneuver regime recognition development and verification for h-60 structural monitoring," in Proceedings of Annual Forum Proceedings-American Helicopter Society, 2007.
- [7] R. Teal, J. Evernham, T. Larchuk, D. Miller, D. Marquith, F. White, and D. Deibler, "Regime recognition for mh-47e structural usage monitoring," in Annual Forum Proceedings-American Helicopter Society, vol. 53, pp. 1267–1284, 1997.
- [8] D. Lombardo, "Helicopter flight condition recognition: A minimalist approach," in Australian Joint Conference on Artificial Intelligence, pp. 203–214, Springer, 1998.
- [9] U. Kalkan, M. Senipek, and A. Yucekayali, "Markovian approach for learning based flight condition recognition methods," in 8th Asian/Australian Rotorcraft Forum, 2019.
- [10] F. Zinnari, G. Coral, M. Tanelli, D. Cazzulani, A. Baldi, U. Mariani, and D. Mezzanzanica, "A multivariate time-series segmentation framework for flight condition recognition," in IEE Transactions on Aerospace and Electronic Systems, vol. 59, no. 3, pp. 2451–2463, June 2023, doi: 10.1109/TAES.2022.3215115.
- [11] <https://leonardo.canto.global/b/IP7IQ>

VERTIFLIGHT TECHNOLOGIES IN LEONARDO

Flight Condition Recognition, Simulation, System Design,
Tilt-Rotor technologies and System Integration



Developing and Applying Means of Compliance for a Powered Lift Aircraft

Luca Belluomini, Joseph M. Schaeffer, Dr. Damian Rogers

Leonardo-Helicopters Division

Modern powered lift aircraft are highly integrated systems that require careful design to guarantee the highest degree of safety and reliability in accordance with existing airworthiness standards. The next generation of powered lift aircraft focuses heavily on reducing pilot workload through fully Fly by Wire control systems. The following article presents design features unique to the AW609, developed to comply with the regulations outlined within the certification basis. Given its tenure within the industry, the AW609 can be used as a case study to show the development of and rationale for safety standards and Means of Compliance, by demonstrating that powered lift aircraft with advanced flight control functions designed for crew workload alleviation provides an equivalent level of safety to existing transport category rotorcraft standards. The article provides the reader with examples of how regulations have been reflected in the design solutions.

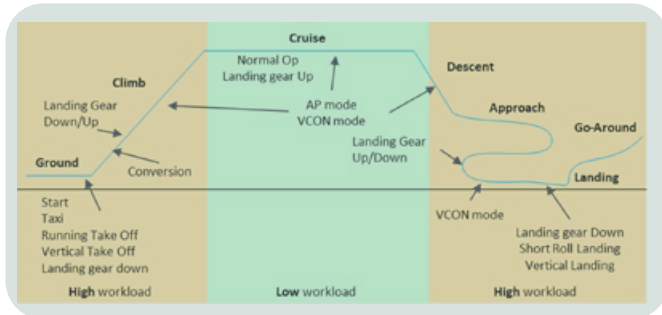
INTRODUCTION

Leonardo Helicopters has collaborated with the Federal Aviation Administration (FAA) to address the unique safety concerns associated with advanced flight control functions required from a Powered Lift (PL) Aircraft (A/C), by publishing over twenty Method of Compliance Issue Papers, effectively evolving airworthiness standards for the AW609 Certification Basis. To successfully decrease the pilot workload and increase the overall safety, automated functions must be carefully designed and implemented, ensuring proper crew situational awareness, especially for non-standard operating conditions such as full or partial system/subsystem failures [2].

The methods of compliance necessary to guarantee adherence to regulations and certification standards must be clearly defined. Means of compliance (MoC) are the detailed design methods employed in practice to demonstrate compliance with regulatory requirements. It is essential to clarify the difference between the two. A *Means of Compliance* is the precise strategy employed to satisfy airworthiness requirements and safety regulations whereas a *Method of Compliance* is the plan orchestrated to demonstrate how feasible

a means of compliance is, such as a ground test, flight test, etc. For example, a *Means of Compliance* could be creating a control loop that compensates for wind in hover. The corresponding *Method of Compliance* could be a flight test in which the centre of gravity must remain within a circle of 5-foot radius. The following article takes a dive into the Fly-by-Wire (FBW) Flight Control System (FCS) design features that are implemented as a *Means of Compliance* to unique PL and FBW FCS regulations specifically pertaining to the AW609. FBW FCS aircraft can be categorized by their fully electronic control infrastructure operated by a computer. This is the essential component in reducing pilot workload. Figure 1 depicts certain flight phases during which increased crew workload is more common whether it be a direct result of system/subsystem malfunction or atmospheric disturbances.

Advanced flight controls are employed to automate various in-flight tasks with the intent of reducing the pilot workload and improving comfort for passengers. With more room to work, pilots can direct their attention to the more difficult aspects of flying such as flight planning, navigation, communication with Air Traffic Controllers, monitoring weather conditions, fuel management, emergency procedures, etc.



1 – AW609 Flight Phases Categorized by Required Pilot Workload and Flight Operation

Aircraft Characteristics

The AgustaWestland AW609 is an entirely FBW tiltrotor (TR) that is poised to change the face of civil aviation. It can lift off vertically, and by tilting its nacelles forward, can convert to fly forwards; providing a speed and range advantage over conventional helicopters while simultaneously offering accessibility and manoeuvrability advantages over conventional airplanes. Specifically pertaining to the AW609, the FBW design consists of a triple-redundant system operating on a two out of three structure. Three flight control computers (FCC) run the same control algorithm simultaneously.

The FCCs process signals and create the appropriate commands if -and only if- at least two out of the three computers return identical results. The AW609 is an example of a highly integrated PL aircraft that alleviates crew workload with unique capabilities, including:

- thrust power management (via tactile cueing),
- full time rotor speed governor including automatically controlled variable RPM,
- auto-trim,
- attitude hold,
- turn coordination,
- flapping limiting,
- nacelle synchronization,
- automatic nacelle control,
- control margin awareness,
- conversion protection,
- stall warning, and “envelope protection” through active control and cueing like: Rate-Of-Descent (ROD), Vortex-Ring-State (VRS), VCON, VMIN and Sideslip.



2 – AW609 Characteristics and Capabilities

Automated functions must be carefully designed to ensure proper crew situational awareness, especially for non-standard operating conditions, including system failures.

Across four prototypes, the first-of-its-kind A/C has flown 2,000+ hours in development and “show compliance” flights. In doing so, it has passed major structural and fatigue tests, critical safety flight tests, vendor component qualification and system safety assessments. The AW609 is designed to meet rigorous FAA commercial transport A/C requirements that provide an additional level of safety above and beyond part 23 and 27 requirements. The AW609 is designed for Category A performance operations, making use of both vertical and short take-off and landing methods (V/STOL). It is equipped to maintain safe operation at all weather conditions. Figure 2 highlights some of the AW609’s capabilities.

Certification Basis

A unique challenge arises in defining the certification basis [1]. As most certification bases are adopted and adapted from those of pre-existing A/C, the AW609’s cutting edge design puts it at a disadvantage. The appropriate combination of existing airworthiness regulations must be chosen, while new special requirements must be clearly defined, which ensure that the tiltrotor’s workload reduction capabilities are certified. There is a level of safety established in the pre-existing applicable sections of existing airworthiness regulations that must be met.

Terms for a brand-new certification basis must be agreed upon, between the industry and regulators, to facilitate the AW609’s certification and set the example for all the emerging tiltrotor A/C. Regulations applicable to airplanes cannot simply be merged with those applicable to rotorcraft. A new set of regulations must be constructed to bridge the gap between the increased manoeuvrability provided by a helicopter and the increased range and airspeed provided by an airplane. The AW609 certification basis is a G-1 Issue paper developed under the 21.17(b) special class regulation [3].

VERTIFLIGHT TECHNOLOGIES IN LEONARDO

Flight Condition Recognition, Simulation, System Design,
Tilt-Rotor technologies and System Integration

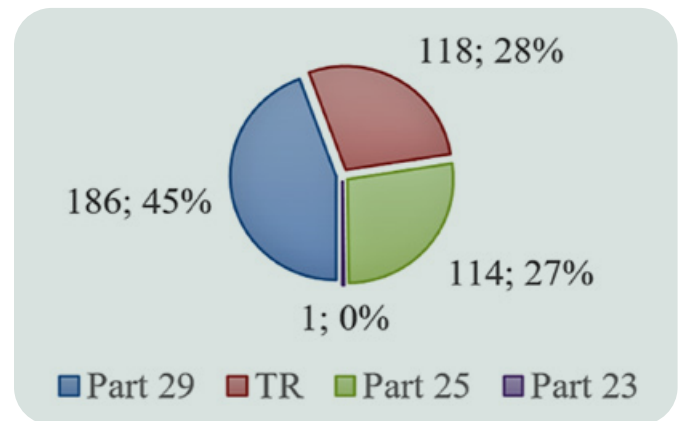
The G-1 issue papers establish the airworthiness and environmental requirements necessary to achieve FAA Type Certification. The Part 21.12(b) of the FAA's Title 14 specifies that for, "special classes of aircraft for which airworthiness standards have not been issued... the applicable requirements will be the portions of those other airworthiness requirements contained in Parts 23, 25, 27 and 29 found by the FAA to be appropriate for the aircraft and applicable to a specific type design" [7][8] and [10].

To avoid any ambiguity, the AW609 certification basis includes new Tiltrotor (TR) airworthiness requirement criteria, i.e. §TR.XX. These newly generated requirements address the unique design and performance aspects specific to the tiltrotor. Some TR airworthiness criteria consist of combined and/or modified regulations from parts 23, 25, and 29, while others are entirely new requirements that are necessary to provide the appropriate level of safety for the AW609.

The initial Type Certificate application was submitted in February 1996, but it had been not accepted for another 6 months after revisions had been made that have led to the third version of the application.

The Certification basis acts as a living document, with adjustments being made constantly as the FAA continues to learn more about the design and characteristics of the A/C. As it currently stands, the certification basis includes regulations from parts 25 and 29, as well as the new tiltrotor airworthiness criteria. Figure 3 portrays the contributions from each part as a quantity first, followed by a percentage.

With such similar requirements, redundancy can be common. In those cases in which redundancy occurs, the most conservative requirements is applied.



3-AW609 Certification Basis Makeup

POWERED LIFT MEANS OF COMPLIANCE

Contrary to the traditional mechanically linked flight controls that provide direct control in all attitudes and manoeuvres, an FBW FCS relies on a flight control computer to process signals from the pilot inceptors and generate electrical signals to command the aircraft. The PL aircraft at hand requires an advanced FBW FCS to translate pilot inputs into engine power and rotor speed, to effectively control moments about all the three vehicle axes.

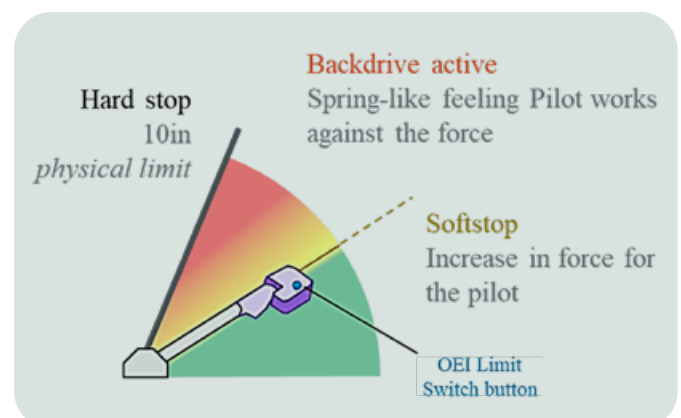
Traditional FCS aircraft disengage or downgrade the level of control when certain limits are exceeded, but it is not possible to completely disengage an A/C FCS, given the premise of an FBW system. However, specific system failures could degrade the FCS. To adhere to §TR.34 & §TR.38, the effects of its design on the system or on the pilot's ability to recover the FBW A/C within the normal flight envelope, must be shown. §TR.34 & §TR.38 pertain to A/C failure states and avoidance of hazardous flight conditions, respectively, and mandate that the effect of the FCS design on recovery ability must be shown.

Thrust Power Management System

The AW609 Thrust Power Management System (TPMS) is a highly integrated portion of the FCS responsible for the engine and rotors. The A/C is equipped with two Pratt and Whitney PT6C-67/A engines designed to operate at all nacelle angles. Engine control and rotor control laws are contained within the FCCs and operate through electronic interfaces with these respective components.

The pilot controls power by using a Power Lever, designed similarly to a helicopter's collective stick. Figure 4 shows a diagram that explains the operation of the power lever.

A power lever has been implemented in the design as it is



4-AW609 Power Lever Functions

A power lever has been implemented in the design as it is difficult to get in and out of the right seat with a V-22 style thrust control lever in place [4]. Additionally, adopting helicopter controls design can allow for reduced pilot training requirements and better alignment to the §TR.779 & §TR.1309. The §TR.779 defines requirements for cockpit controls design, while the §TR.1309 requests rotorcraft equipment and systems to be installed to ensure safety and reliability under any conditions.

The tiltrotor's propulsion system is of high importance for operation and safety of the aircraft, as it provides both lift and manoeuvrability through the drive train.

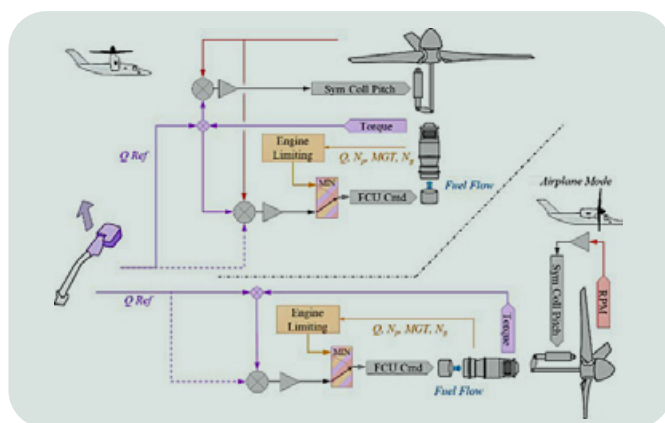
The AW609 TPMS faces a unique challenge as it is designed to meet part 25 and 29 requirements. Part 25 pertains to regulations set on transport category airplanes, while part 29 correlates to the FAA's policies on transport category rotorcraft [9][11].

This is challenging, because helicopters typically use different means to control the rotor speed. In helicopters, the pilot commands the blade collective pitch and the system commands engine power to maintain the desired rotor speed. However, in turboprop A/C, the pilot controls the engine by acting on the throttle command, and the governing system adjusts the required pitch to control the propeller speed. Applying this configuration to helicopters would result in sluggish airframe response. Testing of various strategies during AW609 development indicates that high loads result from mild inputs and the over-torquing/windmilling is difficult to prevent. The §TR.33 requires that the upper and lower operating boundaries of powerplant-generated lift or thrust must be identified.

Figure 5 shows a simplified TPMS response scheme implemented in the AW609 FCCs. A torque loop is added to the scheme to prevent a static instability that would occur when trying to control both the available and the required power by using the rotor speed. In airplane mode, rotor speed is controlled only via the blade pitch angle and torque is controlled by the engine power. In helicopter mode, the two control variables are combined. This scheme provides an optimal combination between characteristics of helicopter and airplane.

Figure 6 depicts the regular engine (Torque Command and Regulation System) and rotor control loop of the AW609 FCC. The combination of rotor speed and torque control reduces the workload during One Engine Inoperative (OEI) operation, particularly for transport operations [5], in response to the §TR.53 & §TR.85 which define requirements for take-off and balked landing, respectively.

The control scheme shown in Figure 6 allows for predictable control sensitivity, reduced transmission over-torque, automatic OEI compensation in all flight modes as requested by §TR.38, and the ability to “set and forget” torque which significantly reduces the workload when converting, and automatically compensates for rotor inflow and altitude changes on torque. The engine control laws oversee managing and displaying engine states, while executing the engine’s control functions.



5-Simplified TPMS Schematic

The system increases the power lever friction when commanding high symmetric torque to cue the pilot when power is beyond the engine limits. This specific design functions as a MoC with the STR.1309.

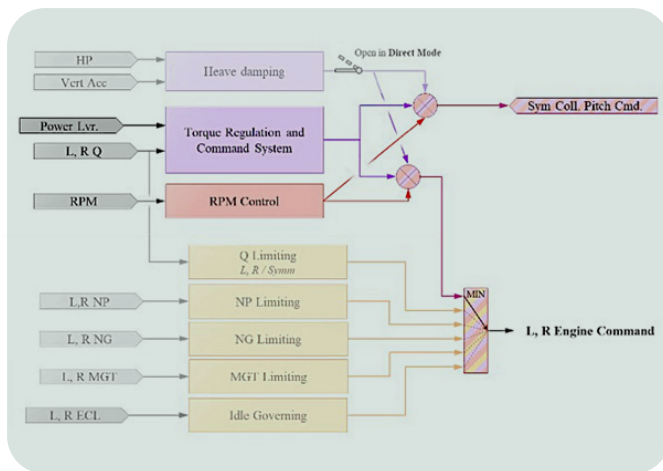
The engine torque limiting function restricts each engine torque based on the flight mode and preserves the drive train lift during all-engine operative modes, by setting a limit requested in §TR.38. The torque limiting is disabled when the engine torque sensors fail and it has limited authority to ensure the A/C effects meet the safety criteria outlined in §TR.1309. The Engine Temperature Limiting function limits the engine temperature, according to the current flight mode. The function has authority limits to prevent from hazardous effects of erroneous sensor operation and is disabled upon detected failure aligning with §TR.33, §TR.38 & §TR.1309.

The Engine Load Sharing Function allows the pilot to match the engine torque or the temperature, to optimize the performance without compromising the ability to attain maximum engine power within limits, effectively satisfying STR.38. The Load Sharing is deactivated in case of failure of either sensors or the interconnected drive shaft (ICDS), to prevent from hazardous effects, as it is directed by STR.1309.

The Engine Failure Detection Function generates a power-off condition that informs avionics to provide a cockpit warning and to enable OEI limit displays in accordance with STR.34, STR.38 & STR.1309.

VERTIFLIGHT TECHNOLOGIES IN LEONARDO

Flight Condition Recognition, Simulation, System Design,
Tilt-Rotor technologies and System Integration



6-Simplified TCRS Schematic

Full Time Rotor Speed Governor

The PL A/C introduce a unique safety consideration pertaining to rotor speed command and control. Failure of this system could compromise the thrust generation and vehicle controllability, thus it could be a catastrophic event. Human error, including errors by flight crew, contributes to more A/C accidents than any other single factor. Such errors can be induced by poorly designed human-machine interfaces that cause inappropriate crew reactions, particularly during flight conditions that demand for increased workload and in emergency scenarios. Airworthiness regulations, design criteria, and MoCs need to be established for PL A/C with automated flight controls, to ensure operational safety in normal and improbable flight conditions, including failure modes.

Automatic control of rotor speed as a function of flight condition serves to reduce the pilot workload. This technology would allow the crew to shift their focus away from managing physical aspects of the A/C, to the mission management, including propulsion system failure conditions.

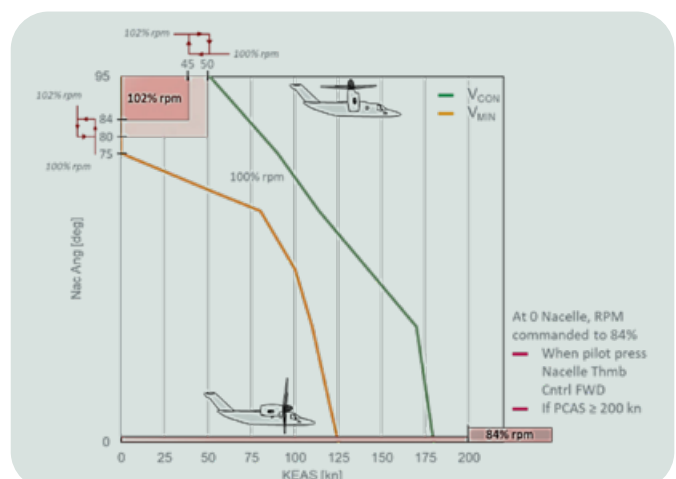
The rotor speed governor function reduces workload for power off operations such as nacelle reconversions, per §TR.143 which requires that the A/C must be safely controllable and manoeuvrable during steady flight and appropriate manoeuvres. The governor automatically reduces the collective pitch to maintain the rotor speed, thus relieving the pilot from the need to react to an engine failure, by reducing the power lever to enter VTOL mode or Airplane Mode. The envelope protection function provides a means to keep the rotor speed (N_r) within the design limits and it is designed to satisfy the N_r Over/Under-speed Protection requirements, as discussed in §TR.38. The cockpit displays indicate the rotor speed operation limits to the pilots and provide a WARNING when they are violated, aligning with §TR.1309.

Airplane Mode refers to the A/C configuration with nacelles on the downstop (0° nacelle angle) and rotors at 84% of their nominal rotor speed. The AW609 FCS includes a sensor that detects when the nacelles are positioned horizontally.

All other flight modes, with nacelles tilted at various angles (0° to 95°) and the rotor at 100% or 102% the nominal rotor speed, are referred to as VTOL/Conversion Mode (V_{CON}). This relationship is shown in Figure 7.

The TPMS can temporarily disable the Full Time Rotor Speed Governor, to allow rotor speed to drop under the intended reference speed in specific conditions, adhering to §TR.34. The limits on the collective pitch command are enforced on the Collective Governor that computes the desired collective blade pitch value to maintain a specified RPM/Torque reference. The lower limit allows the pilot to maintain some authority on the collective pitch when the governor works against him and tries to accelerate the rotor by lowering the blade pitch.

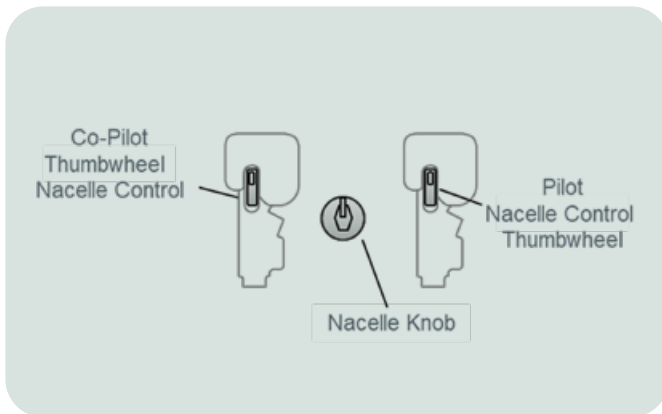
In cases in which the system detects the power degraded situation - like: OEI, All Engines Inoperative (AEI), fuel contamination or engine ingestion - the lower Collective Governor limit can be overridden by the pilot through a rapid, large power lever movement. This provides added safety margin by cushioning a hard landing in a power-limited emergency [6].



7-Rotor RPM Command Logic

Nacelle Control

In accordance with §TR.53 through §TR.85, the Nacelle Angle positioning is ensured by the nacelle angle control. These requirements are primarily concerned with flight performance, during which the nacelle control is crucial. The requirements specify the absolute minimum standards for performance in each flight scenario. The nacelle wheel and its location on the power lever is shown in Figure 8.



8–Nacelle Wheel

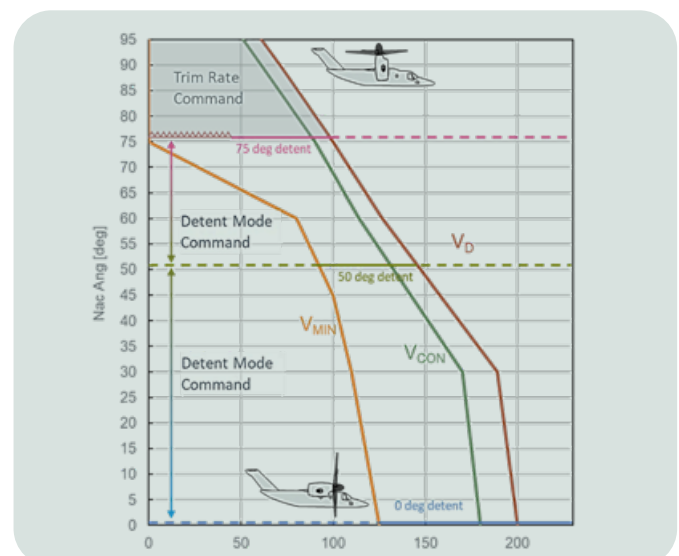
The Nacelle angle control provides continuous control in/near helicopter mode (95° to 75°) at a fixed rate. The capability to command conversion rates of ± 8 degree/s for any nacelle position in helicopter mode is provided. When approaching 95 degrees, the command is reduced to 1 degree/s. The nacelle manual trim control allows the pilot to set any nacelle angle between 75° and 95° in a smooth and predictable manner. Nacelle angle control provides semi-automatic detents (75° , 50° , downstop) for converting at pre-programmed fixed rates of ± 3 degree/s. The nacelle angle control function operates smoothly such that the nacelles stop at each detent and wait for another nacelle switch command to initiate further nacelle motion.

The Nacelle angle control provides a high-speed emergency reconversion mode that over-rides detents. The Emergency Reconvert Function requires a single action to command nacelles to 95 degrees, unless it were inhibited by the conversion protection. The Nacelle angle control stops the commanded motion when nacelles are commanded in the direction opposite to current motion. The command nacelle angle is changed at a rate schedule selected to give Satisfactory Handling Qualities for conversion and reconversion. The Nacelle angle control limits the nacelle angle to above 75 degrees when on the ground with rotors turning, and provides bang-bang nacelle rate control at 2 deg/sec when on the ground with low rotor RPM. In control theory, the bang-bang control (hysteresis, 2-step or on-off control) provides feedback to the system and enables rapid transitions between the two states. The quick transitions enabled by the implementation of such control strategies is especially important in systems in which the response time must be shortened as much as possible. During the conversion to the downstop, the rate of change of the nacelle position command is reduced to 1 degree/s within 2 degrees of the downstop.

Airspeed Definition

A tiltrotor has new forms of envelope restrictions that are introduced by its moving nacelles. The AW609 uses various techniques to cue the pilot to the A/C operating envelope. A conversion corridor represents the protection control laws that are intended to allow the pilot to easily keep the A/C within the nacelle vs. airspeed limits.

Flying the tiltrotor within airspeed limits helps to reduce the fatigue and increase lifespan of the rotor system components. Figure 9 portrays the nacelle control scheme and conversion corridor definition in power ON modes. Considering the conversion corridor boundaries, the lower and upper limit speeds in VTOL/Conversion mode are called V_{MIN} and V_{CON} as it is prescribed by §TR.11. This is a relatively new concept for civil A/C, but a proven one that the V-22 community is already familiar with.



9–Nacelle Control and Conversion Corridor–Power ON

VERTIFLIGHT TECHNOLOGIES IN LEONARDO

Flight Condition Recognition, Simulation, System Design,
Tilt-Rotor technologies and System Integration

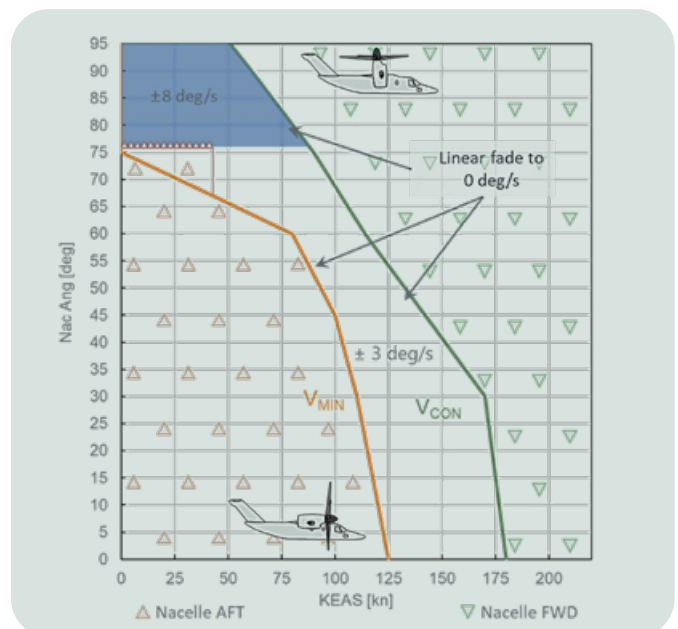
Flying below V_{MIN} or above V_{CON} induces large flapping angles on the gimbaled proprotor system, which can lead to higher temperatures of the elastomeric bearings and to reduced life spans.

With engines operating, the FCS sends V_{CON} to the avionics processor for display and over-speed aural warning, which is required by §TR.38 on the avoidance of hazardous flight conditions. A power-off operating speed has been established, as per §TR.1505, to allow AEI reconversions and high speed autorotation. All-engines-out logic causes the FCS to switch, sending the power-off airspeeds in accordance with §TR.34 in the event of any critical propulsion system failures.

Conversion Protection

The nacelle conversion protection Control Laws structure relies on the limitation of the nacelle rate applied to the command. The limits are such that in normal operations the nacelle command would never exceed the Computed Airspeed (CAS) vs Nacelle Angle envelope known as the conversion corridor. These limits directly correspond to both §TR.33 and §TR.38. Figure 10 shows the conversion protection scheme outlined by the control algorithm.

The conversion protection function limits the nacelle rate in the direction that, based on the desired nacelle angle and airspeed, could bring the A/C into a dangerous flight condition. The upper limits are chosen with respect to the potential of structural damages, while the lower limit selection is due to the possibility of sustaining the level flight in that condition. Areas outside the conversion corridor allow for nacelle movements in only one direction, as it is detailed in Figure 10. The commanded nacelle rate is not sharply brought to zero at the edge of the corridor, but it linearly fades to null as a function of airspeed. While the airspeed is approaching the intended limit, the system produces visual and audio cues to increase the pilot awareness. Note that when the pilot moves the A/C back into the conversion corridor, i.e. accelerates or decelerates sufficiently, then the nacelles will start moving forward or aftward again without prompting from the pilot. In the area below 45kts and 75deg, conversion forward is not allowed at any time.



10 – Conversion Protection

This logic prevents the pilot from tilting the nacelles forward too early and losing lift from the rotor system (by tilting the thrust vector forward) before there is any lift being generated from the wing surfaces. Autoflaps and longitudinal control processing is designed to minimize pilot workload to remain within the conversion corridor during nacelle transition maneuvers.

As per §TR.34 on the failure of critical propulsion systems, conversion protection is disabled when the FCS reverts in DIRECT mode or the Power Off situation is detected. The Control Laws operating in the DIRECT mode provide a system which is adequate for continued safe flight and landing. This mode is entered only following a failure which prevents operation in the NORMAL mode. Transition from NORMAL to DIRECT mode may occur automatically as a function of detected system failures or manually by the pilot in the event of an undetected failure by switching the “FCS AUG” switch to the OFF position. The Control Laws detect the Power Off when any two out of the left engine, right engine or Interconnected Drive Shaft fails.

CONCLUSIONS

The AW609 Certification Basis for FAA Type Certification Project #TC3419RC-R is an evolution of the initial certification basis which was released in September 2007 under “Proposed Airworthiness Standards, Request for Comments” which encompassed a mix of new tiltrotor requirements and existing regulations from Parts 23, 25, and 29.

The previous proposal was culminated over 20 years of industry development led by the FAA, which started as an interim airworthiness requirement for powered lift A/C called 'Part XX' and evolved through a collaborative effort. The recent update includes modifications to address the updated part 25 airworthiness requirements and the unique §TR.XX airworthiness criteria provided to AWPC. The updates address special conditions deemed appropriate by the FAA based on over 2000 hours of flight test, thousands of hours of simulation, and extensive collaboration between industry and the FAA. The process and results described in this paper are mature. The current version of the AW609 certification basis is undergoing final reviews and approvals for public release in 2023 as the G-1 Issue Paper for Project #TC3419RC-R.

Luca Belluomini: Luca.Belluomini@leonardocompany.us

REFERENCES

- [1] King, David, Mcallister, Robert, and Arifian, Kenneth, "Civil Certification Methods for Advanced Rotorcraft Flight Control Systems," American Helicopter Society 60th Annual Forum Proceedings, Baltimore, Md, June 2004
- [2] USHST, "Loss-of-Control In-Flight Mitigation through Installation of Stability Augmentation and Autopilot Systems in Light Helicopters," February 2021.
- [3] FAA Issue Paper G1, (AW609 Certification Basis)
- [4] Cullen, Lachlan and Schaeffer, Joseph "Operating Procedures and Control Laws for Transport Category Performance in the Bell-Agusta 609 Tiltrotor" American Helicopter Society 63rd Annual Forum Proceedings, Virginia Beach, VA May 2007
- [5] Schaeffer, Belt, Campbell, Mattaboni, and Colombo, "Development and Testing of Transport Category Vertical Takeoff Procedures for the AW609 Tiltrotor," American Helicopter Society 71st Annual Forum Proceedings, Virginia Beach, VA May 2016.
- [6] Wells, Dan, and Edwards, Paul, "Development and Testing of AW609 All-Engines-Inoperative (AEI) Emergency Re-conversion," 71st Annual Forum of the AHS, Virginia Beach, VA, May, 2015
- [7] Title 14, Code of Federal Regulations Part 21, section 21.17, Designation of applicable regulations
- [8] Title 14, Code of Federal Regulations Part 23, Airworthiness Standards, Normal Category Airplanes
- [9] Title 14, Code of Federal Regulations Part 25, Airworthiness Standards, Transport Category Airplanes
- [10] Title 14, Code of Federal Regulations Part 27, Airworthiness Standards, Normal Category Rotorcraft
- [11] Title 14, Code of Federal Regulations Part 29, Airworthiness Standards, Transport Category Rotorcraft

VERTIFLIGHT TECHNOLOGIES IN LEONARDO

Flight Condition Recognition, Simulation, System Design,
Tilt-Rotor technologies and System Integration



Automated Robotics for Testing Optimization: an Automatic System for Cockpit Integration Testing

Vincenzo Taumaturgo¹, David Frisini², Giorgia Giulianini², Marco Romano²,
Nicola Zonzini², Glauco Rinaldi²

¹Leonardo – Helicopters Division, ²TXT e-Tech

The purpose of this paper is to report the results of the evaluation conducted on Automated Robotics for Testing Optimization (ARTO), an automated system designed to perform integration tests requiring interaction with the cockpit. The system features two key elements: the robotic manipulator that acts on cockpit panels and displays, and the Computer Vision that collects the visual information. The methodology followed during the activity addressed different System Engineering technical processes, starting from the architectural design of the system, up to the validation in a representative testing environment. For the validation environment of ARTO, TXT E-Tech, and Leonardo Helicopters have chosen the LHD Next-Gen Civil Tiltrotor-Technology Demonstrator (NGCTR-TD) Avionics Full Scale Integration Rig (FSIR). The results collected during this activity include several KPIs, significant in terms of accuracy and test operation efficiency.

INTRODUCTION

This section introduces the Automated Robotics for Testing Optimization (ARTO) solution, developed to enhance the integration testing and the procedures automation.

Within the aerospace industry, integration testing is one of the steps that compose the system development life-cycle, well depicted by the V-model [1]. In general, the V-model is used for the complex systems design & development, through physical levels of solution description, and physical realization of system elements, along with their integration to create higher physical level system elements, [1].

For the integration testing of an avionic system, many different scenarios must be executed and validated by the user running the test, and either with the current state of the art of integration testing, test executors make several repetitive actions [14].

The test sets of safety-critical systems are long lasting and involve repetitive tasks for the operator.

Meanwhile the system is under test, the laboratory cannot be used for other purposes, which decreases the asset's availability for other stakeholders. Moreover, with distributed offices, the on-site testing could be constricting when the execution of test procedures requires at least one person physically attending in the laboratory [2].

ARTO addresses the abovementioned problem by automating the repetitive procedures in which human interactions are required, to increase efficiency, reduce costs and enable working remotely from different locations.

The system consists of four main subsystems: Robotics, Image & Audio Processing (Computer Vision), Framework, and User Interface. ARTO is designed to be installed in a generic cockpit, whether it is located in a real helicopter/aircraft or a testing laboratory, with the aim to enable the key technology of automatizing human procedures for relevant purposes.

IMPLEMENTATION

As shown in Figure 1 and detailed in Figure 2, the four main subsystems implemented are: Graphical User Interface (GUI), Framework, Robotics and Computer Vision (CV).

All subsystems are implemented and integrated within a Robot Operating System (ROS), that consists of a set of software libraries and tools designed for building robot applications. This robotic middleware uses a graph-based architecture to divide tasks among multiple nodes that are managed as individual processes that communicate through messages, services, or actions [11].

Framework

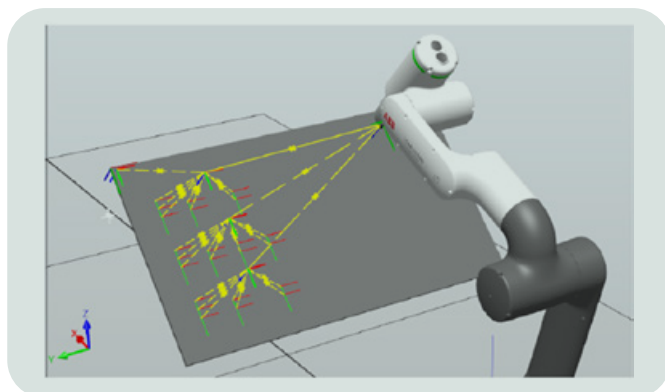
The Framework is the software that manages the connection among all the subsystems [4]. The main features the Framework subsystem shall implement are:

- Initiate the subsystems;
- Manage the subsystems and their integration;
- Distribute tasks to different subsystems;
- Execute tests;
- Notify each subsystem of a test execution;
- Manage the results.

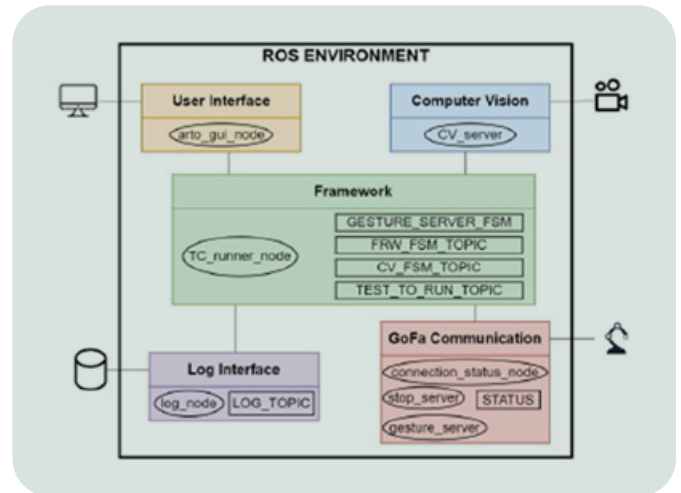
Robotics

As described in [3], the Robotics subsystem is composed by a robot that interacts with the cockpit and stimulates the system under test. The main features that the Robotics subsystem shall satisfy are:

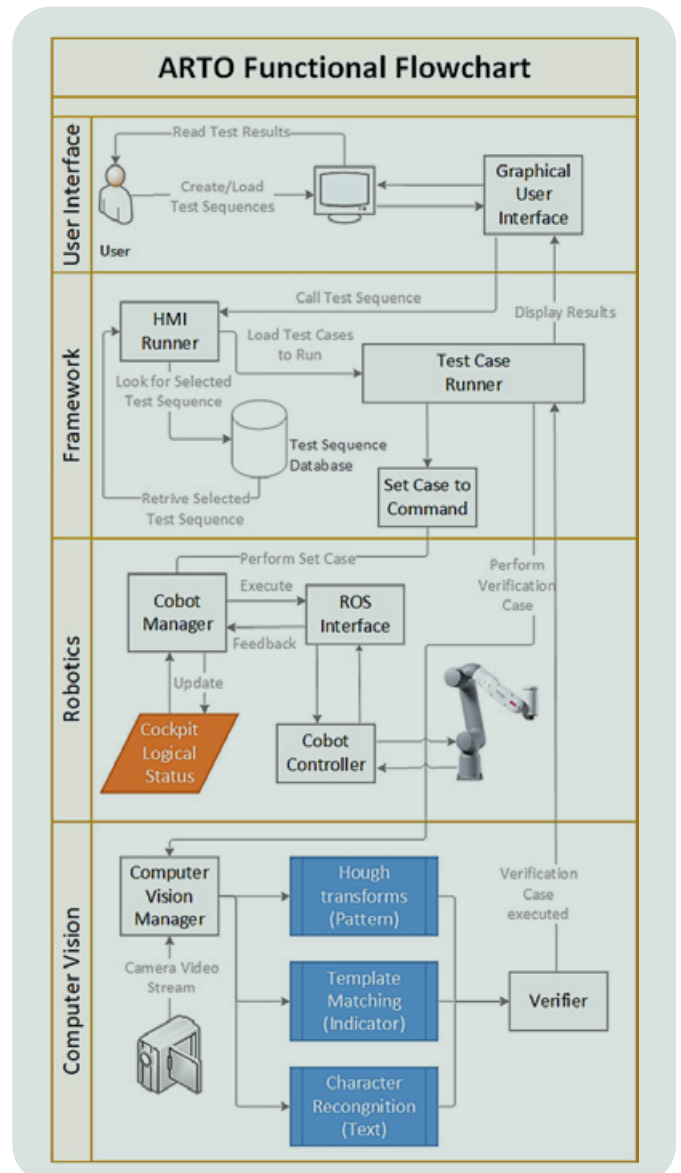
- The robotic arm does not represent a threat to humans who share the working environment with it;
- The robotic arm is capable of operating on the touchscreens, push buttons and levers;
- The robotic arm is designed to be easily installed and removed from the cockpit, allowing the cockpit to be reconfigured quickly for other needs or for maintenance.



3–Trajectory planning in RobotStudio



1–Robot Operating System environment



2–ARTO Functional Flowchart

VERTIFLIGHT TECHNOLOGIES IN LEONARDO

Flight Condition Recognition, Simulation, System Design,
Tilt-Rotor technologies and System Integration

As the robot must be safe both for the humans who operate it and for the environment, a cobot (collaborative robot) has been evaluated, since it has been developed precisely for this purpose. The final choice was the ABB (ABB Asea Brown Boveri Ltd) GoFa™ CRB 15000 launched in 2021, that requires no specialized training to use and is light enough to be moved and installed on-site easily.

The first integration studies have been conducted in RobotStudio, a software developed by ABB that allows developers to create a digital representation of the robot and its operational environment as shown in Figure 3. It has been used to simulate different scenarios and test the system's capabilities in a safe and controlled digital environment [5].

Computer Vision

The Computer Vision subsystem aims to replace the verification step performed manually by test engineers. The subsystem is composed of a camera and software module used to analyse information from the cockpit elements. The main features the Computer Vision subsystem shall implement are:

- Recognize the buttons, levers, or knobs to operate;
- Recognize if a certain indicator is displayed in the field of view of the camera;
- Recognize if a button has been correctly pushed.

About the hardware, A Raspberry Pi 4 single-board computer [13] has been chosen, equipped with a Camera Module and suited with several software tools to allow the extraction, packaging, and broadcasting of images, thus providing a real-time stream of data packets to the image processing algorithms embedded in the Framework. The software developed includes a pre-processing phase, aimed to enhance quality of the frame and to reduce noise, also performing various image operations such as colour filtering, morphological manipulation, and smoothing.

The final goals of object detection, recognition, and tracking have been achieved through implementation of Template Matching algorithms [6] and Hough Circle Transform (HCT) method [7][12], used to detect circles in an image by eroding and removing the elements of the Region Of Interest (ROI) [8].

Graphical User Interface (GUI)

The GUI allows the user to manage the functions of ARTO and lets the operator to design, execute, and collect/review the results of the specific test.

The main features the User Interface subsystem shall implement are:

- Intuitive and easy-to-use interface to create, save, and load test scenarios;
- Real-time feedback on the status of every subsystem during test execution;
- Error handling and reporting features for efficient debugging and problem-solving.

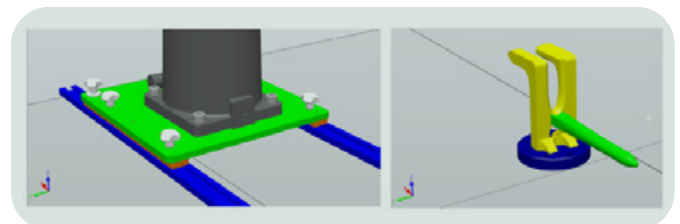
Hardware Installation

The installation provisions include the base used to install the robot, the tool applied to the robotic arm and the hardware connections. The base provision has been designed to be installed on the cockpit pilot seat rails, as shown in Figure 4 (left).

This has been done in order to allow for quick installation with minimum impact on the cockpit (only seat removal is required), at the same time allowing precise positioning of the robotic arm, and optimal position in terms of reachability of displays, buttons and levers.

The tool applied to the robotic arm has been optimised for pressing operation on a touch-screen display and a pulling operation on the landing gear lever.

With reference to Figure 4 (right), the tip of the green section is aimed to press the touchscreen displays, hence it has been covered with soft rubber material in order to avoid potential damage to the screens, whereas the yellow part is designed to pull and raise (or lower) the landing gear lever.

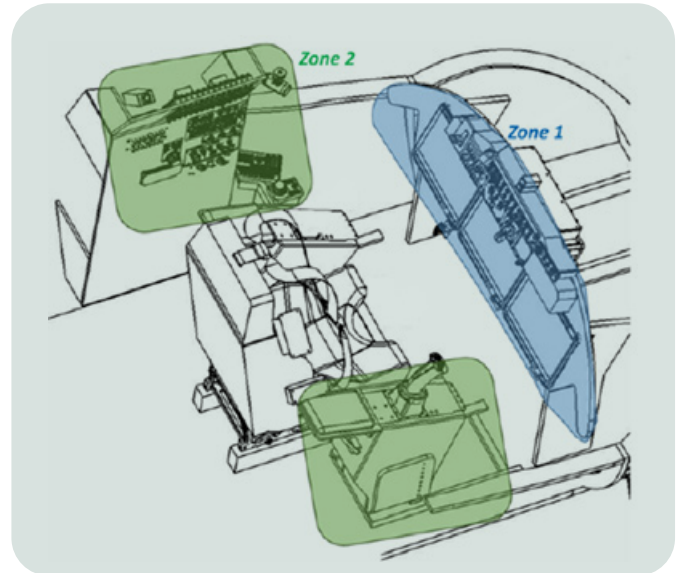


4 – Base provision and grip tool

VALIDATION TESTS

The operational capabilities of ARTO have been validated within a laboratory environment, and used for actual aircraft vehicle testing activity. Such laboratory environment is the LHD Next-Gen Civil Tiltrotor-Technology Demonstrator (NGCTR-TD) Avionics Full Scale Integration Rig (FSIR) environment, as described in [3] that includes real the Electrical, Avionics and Flight Control systems, including actual hydraulics, along with testing capabilities for all of these systems.

It is worth noting that the NGCTR development program has received funding from the Clean Sky 2 Joint Undertaking (JU) under grant agreement No 945542. The JU receives support from the European Union's Horizon 2020 research and innovation program and the Clean Sky 2 JU members other than the Union. In particular, the Cockpit Mock-up environment included within the laboratory, has been used for the evaluation, by installing the ARTO Robotic Arm in lieu of the pilot seat in the middle of the cockpit.



5-Cockpit Mock-up test environment

This position has allowed for proper reachability of all the real equipment installed in the cockpit main zones, shown in Figure 5. The Instrument Panel (Zone 1) features a flight deck with three wide-format landscape touchscreen displays, along with control panels for Engine and Fire Extinguishing Control Systems.

In addition, the Cockpit Display System also includes dedicated cockpit controls for cursor manipulation, data setting alphanumeric entry and controls for commonly used functions.

Control panels include Cursor Control Panels (CCPs), one Multifunction Keypad Panel (MKP) and one Display Mode Control Panel (DMCP) installed within the side areas (Zone 2), along with the Active Inceptors.

At first, only the CV has been tested, then only the Robotics subsystem separately, and at the end all the subsystems integrated. The executed tests are described hereinafter.

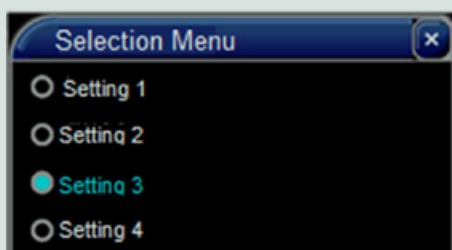
Recognition of indicators



6-Landing Gear Indicators: U&L, Transition, D&L

The Computer Vision has been tested as standalone in this test, aimed to detect the landing gear status indicators depicted in Figure 6: *Up&Locked* (left side), *Transition* (center) and *Down&Locked* (right side).

Moreover, other two customized indicators have been tested, which in this paper are indicated as *Fail Status 1* and *Fail Status 2*. In addition to the Landing Gear Indicators recognition, another test has been performed, aimed to recognize the navigation source menu (example shown in Figure 7).



7-Navigation Source Menu

This latter test consisted in detecting and recognizing the exact position of the setting, depicted by a cyan circle in the menu, as well as the correct number of frames in which the indicator was active (i.e. it didn't detect false positives or false negatives).

VERTIFLIGHT TECHNOLOGIES IN LEONARDO

Flight Condition Recognition, Simulation, System Design,
Tilt-Rotor technologies and System Integration

Touch control push and detection

A complete test has been made with the Crew Alerts Window: the scope was to open it through the dedicated touch control on the screen, and close it with the vertical bar. Moreover, the CV had to detect if the window was expanded or collapsed. This has been achieved by using Template Matching algorithm. Moreover, the complete test (including robot gestures and automatic verification) has been started using the GUI.

User Test

The last test performed was a user test. Namely, a test engineer has been instructed to set a test with ARTO and to execute it for the first time. Setting, execution time and tester opinion have been gathered as a qualitative measure of efficiency of the system.

RESULTS

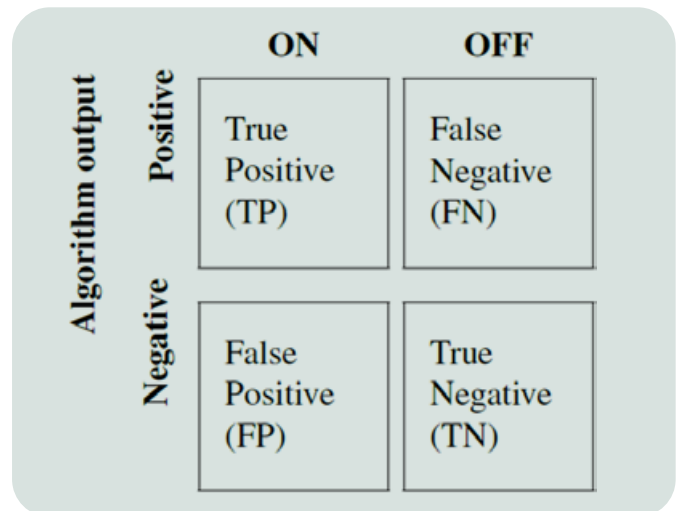
Computer vision results are expressed using the notation in Figure 8, where TP, FP, TN, and FN refer to each processed frame, containing the indicator or not. Moreover, the following KPIs have been recorded for the Computer Vision module test results [9][10]:

- **Accuracy:** $\frac{(TP+TN)}{(TP+TN+FP+FN)}$
- **Precision:** $\frac{TP}{(TP+FP)}$
- **Average Matching:** expressed in percentage of matchings found over the Region Of Interest
- **Frames per Second:** evaluated by the algorithm, an indicator of the processing speed.

The results about the recognition tests: Landing Gear status indicators, Navigation Menu, Expanded Alert Window (named as Window 1) and Collapsed Alert Window (named as Window 2) are reported in the following Table 1.

Test	TP	FP	TN	FN
D&L	100%	0%	0%	0%
Transition	97.7%	2.3%	0%	0%
U&L	96.6%	0%	0%	3.4%
Fail 1	100%	0%	0%	0%
Fail 2	85.3%	0%	14.7%	0%
Red X	100%	0%	0%	0%
Nav Source	18.6%	0%	81.4%	0%
CAS Expanded	100%	0%	0%	0%
CAS Collapsed	100%	0%	0%	0%

Table 1-Results for CV recognition test



8 – CV Results Notation

Test	Acc.	Prec.	Avg. Match	Avg FPS
D&L	100%	100%	96.4%	13.4
Transition	97.3%	97%	91%	12.4
U&L	96.6%	98%	41%	12.4
Fail 1	100%	100%	64.6%	15.9
Fail 2	100%	100%	65%	12.4
Red X	100%	100%	54%	21.3
Nav Src	100%	100%	-	27.2
Window 1	100%	100%	82%	15.7
Window 1	100%	100%	82%	15.7

Table 2-Aggregated KPIs for CV recognition test

Tests results show high consistency among the different features to recognize by the Computer Vision algorithm. The aggregated KPIs are then resumed in Table 2. The average FPS rate processed by the algorithms is about 14.4 with a minimum of 12.4 FPS and a maximum of 21.3 FPS. The overall accuracy and precision of the recognition is extremely satisfactory, also at lower matching percentage.

This latter value is an indicator of how the algorithm is resilient to noisy input images, and how good is the threshold fixed for the template matching algorithm.

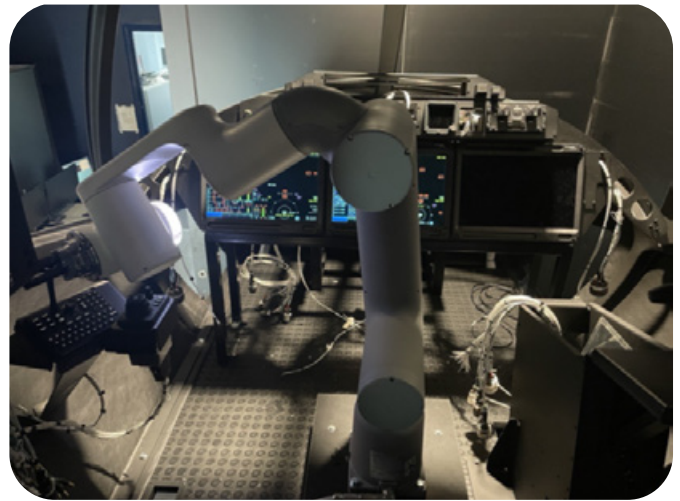


9-Reachability test on Left and Right Display

About the robot operation on the touchscreen, the implemented gesture resulted in an average number of 9 ‘missing clicks’ every 50 touches. Such missing clicks resulted in the grip touching a display area very close to the interactive one, but missing the target hotspot or not pressing enough to trigger the interactive area.

Finally, an ‘User Test’ has been performed, asking an experienced test engineer to implement a test procedure using ARTO for the first time. Such tests has highlighted how the execution time involving the tool is slower than when executed by a human operator. Nevertheless, the time required to write and prepare a test procedure using ARTO, is largely lower with respect to the conventional test preparation method, as shown in Table 3. (see video in [17])

Other KPIs measured with the Reachability Test and the Navigation Source Menu Test are related to the robotic arm. The cobot has been demonstrated itself being able to reach all the displays and push buttons within Zone 1 and Zone 2 as it can be seen in Figure 9 (and related video in [16]) and Figure 10, without any interference with other existing items installed in the cockpit.



10-Reachability test on Zone 2 (Keyboard)

User Test KPI	Human operation	Using ARTO
<i>Familiarization</i>	-	20 min
<i>Test Preparation</i>	15 min	5 min
<i>Test execution</i>	5 sec	30 sec

Table 3 – User Test KPIs

CONCLUSIONS

At the conclusion of the evaluation activity of ARTO within the laboratory environment of NGCTR-TD, it can be stated that the Technology Readiness Level (TRL) reached by the system is TRL 5. The main achievements can be depicted in 3 areas:

- Main capabilities;
- Demonstrated Usability by a typical operator;
- Negligible impact on the installation inside a cockpit.

The two fundamental capabilities that have been analysed with the several tests conducted on the representative environment, are the recognition of the pilot screen indicators and the robot handling capabilities to act on the different panels. For this area, it can be stated that the system has sufficient functionalities implemented to execute the tests in the scope of the activity.

The results of the test conducted with a test engineer using the system for his/her first time, were concluded with positive outcome in terms of the set-up of the system and test management. This evaluation will be re-conducted with future implementation and increase in test procedure complexity. The choice of the installation proved to be a good compromise between repeatable centring of the manipulator position and the use of a fixed cockpit element, namely the seat guides. This has allowed to easily reposition the system even by a single non-trained operator. Of course, the system features also some limits. In the first instance, the number of indicators that can be recognized correctly by the Computer Vision is limited, therefore the type and number of symbols identifiable shall be increased accordingly with the number of the test procedure that will be covered by ARTO.

VERTIFLIGHT TECHNOLOGIES IN LEONARDO

Flight Condition Recognition, Simulation, System Design,
Tilt-Rotor technologies and System Integration

Secondly, the robotics procedures will be optimized in terms of time of execution and gripper design; also in this case, the test procedure will be the driver. In the following section, the details of these future improvements are outlined.

Future Developments

Several future growth capabilities of the system have been identified for each subsystem, to increase the capabilities of ARTO.

The first function the Framework should be able to support, is the aural signal recognition that would enable ARTO to cover integration tests requiring sound verification. Moreover, the Framework should be able also to receive the coordinates of the external environment from the Computer Vision subsystem, to process them, and to send them to the robotic subsystem. This would eliminate the initial calibration procedure of the robotic system during installation and initialization, and result in a more precise gesture execution. The timing between the Computer Vision camera and the Framework subsystem could be improved as well, to make more efficient and faster automated tests involving both Computer Vision and gestures. Concerning the robotic arm, the gripping tool is identified as an improvement area, to ensure the soft pencil tip does not change its shape or position after prolonged usage.

Another improvement that will be analysed, to efficiently reduce the time in test execution, is the robotic gestures speed, while maintaining the safety limitations to avoid any human injuries. Also about this point, another improvement will be teaching the robot entire trajectories, instead of the sole coordinates.

Then, obstacles should be recognized with the use of Computer Vision, and avoided accordingly. Finally, a force sensor could be installed between the robot and the tool, to further verify that the gesture has been completed and to avoid missing click.

About Computer Vision, quality of the camera will be upgraded to reduce the video noise. Having a cleaner image to start with, would reduce the need of using computationally heavy image enhancing techniques.

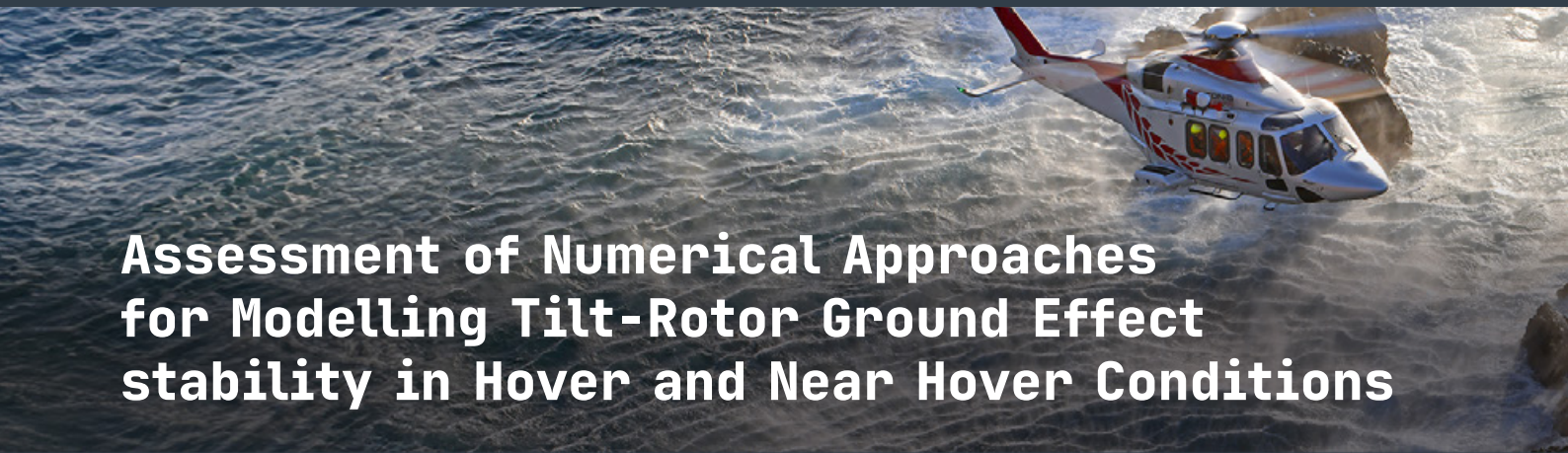
This should allow improvements both in speed and precision of the already existing and future algorithms. Especially, an immediate improvement consists in recognizing automatically the edges of the screen and the Region Of Interest (ROI), without any manual calibration at each time. Other code improvements include also the automatic calibration of the image pre-processing steps (such as masking and morphological operations) according to the environment or lab conditions. Moreover, in order to better test and select CV algorithms, a comparison between Template Matching (kept as the benchmark) and other techniques will be performed. For example, in the Cockpit Display System environment, many textual indicators are used and need to be tested to verify their right behaviour. For instance, the Optical Character Recognition (OCR) could enhance text indicators detection.

The OCR is already being developed, using Google's "Tesseract OCR", and is currently being tested on other indicators not discussed in this paper. Although promising, the tests so far have been run on high-quality images, and thus they are only partially indicative of a real scenario. Moreover, since the CDS uses a particular font, in a particular domain, the development of customized OCR software is being taken into consideration.

Another solution that is under development consists in applying a Convolutional Neural Network (CNN) capable of recognizing both complex indicators (with their associated status) and ROIs [3]. Other Deep Learning techniques, related to CNNs that will be investigated and tested, include the VGG (Very-deep Geometric Group), U-Net and MobileNet, all of which represent state-of-the-art architectures in terms of accuracy and versatility.

REFERENCES

- [1] B. Boehm, "Guidelines for verifying and validating software requirements and design specifications," in Proceedings of the European Conference on Applied Information Technology of the International Federation for Information Processing (Euro IFIP), 1979.
- [2] H. Sartaj, M. Iqbal and M. Khan, "Testing cockpit display systems of aircraft using a model-based approach," Springer-Verlag GmbH, Germany, 2020.
- [3] D. Frisini, V. S. Stotz, G. Morlacchi, V. Taumaturgo, "Technology Concept of an Automated System for Integration Testing", European Rotorcraft Forum 2022. <https://www.rotorcraft-forum.eu/paper-download/>
- [4] Elkady, A., & Sobh, T. "Robotics Middleware: A Comprehensive Literature Survey and Attribute-Based Bibliography". Journal of Robotics, 2012, 959013. <https://doi.org/10.1155/2012/959013>
- [5] JoiintLab (2022). abb wrapper. Accessed March 8, 2023 https://github.com/JOiint-LAB/abb_wrapper
- [6] Asharul Islam Khan and Salim Al-Habsi (2020). "Machine Learning in Computer Vision". Procedia Computer Science, vol. 167, 1444-1451. <https://www.sciencedirect.com/science/article/pii/S1877050920308218>
- [7] Forgo, Z., Villanueva Portela, M. A., Hypki, A., & Kuhlenkoetter, B. (2020). Dual arm robot control by hands gestures using ROS. ISR 2020; 52th International Symposium on Robotics, 1–6.
- [8] Schauer, M., Czekansky, J., Kreutzer, M., & Bienhaus, D. (2022). Robot-based image acquisition for dendrochronological analysis of curved wooden surfaces. ISR Europe 2022; 54th International Symposium on Robotics, 1–6.
- [9] Zhao, F., Huang, Q. and Gao, W. "Image Matching by Normalized Cross-Correlation". IEEE International Conference on Acoustics Speed and Signal Processing Proceedings. 2006.
- [10] Di Stefano, L., Mattoccia, S. and Tombari, F. (2005). "ZNCC-based template matching using bounded partial correlation". Pattern Recognition Letters, vol. 24, 2129-2134. <https://doi.org/10.1016/j.patrec.2005.03.022>
- [11] IBM. (2022). "What is middleware?" Accessed March 10, 2023 <https://www.ibm.com/topics/middleware>
- [12] Rizon, M., Yazid, H., Saad, P. Md Shakaff, A. Y. and Saad, A. "Object Detection using Circular Hough Transform", American Journal of Applied Sciences (vol. 2), 2005, 10.3844/ajassp.2005.1606.1609.
- [13] Michael H. (Laserlicht), "Raspberry Pi 4 Model B from the side.", Image and General description from Wikipedia https://it.m.wikipedia.org/wiki/File:Raspberry_Pi_4_Model_B_-_Side.jpg
- [14] Guidelines for Development of Civil Aircraft and Systems, ARP4754A, 2010.
- [15] Evaluation of an Automatic System for Cockpit Integration Testing - David Frisini, Giorgia Giulianini, Marco Romano, Nicola Zonzini, Glauco Rinaldi (TXT e-Tech), Vincenzo Taumaturgo (Leonardo Helicopters) – 79th Vertical Flight Society Forum.
- [16] <https://leonardo.canto.global/b/PRSF8>
- [17] <https://leonardo.canto.global/b/R5D49>



Assessment of Numerical Approaches for Modelling Tilt-Rotor Ground Effect stability in Hover and Near Hover Conditions

Federico Porcacchia, Fabio Riccardi, Andrea Mancini, Matteo Pecoraro, Andrea Ragazzi, Luca Viganò

Leonardo - Helicopters Division

The paper aims at the synthesis of a ground effect model suited for real time pilot in the loop and design trade-off analyses of tilt-rotor like configurations. The process, based on the outcomes of dedicated Computational Fluid Dynamics (CFD) high fidelity simulations, is related to the determination of analytical model corrections to apply to tiltrotor aeromechanic model suited for out of ground effect conditions. The impact of the proposed modelling approach on the vehicle trim attitudes and bare aircraft stability is then assessed. Finally, effectiveness of the control laws synthesized out of ground effect is assessed in ground effect comparing bare aircraft vs closed loop system root locus. Stability margins evaluated through disk based approach are used to investigate robustness of the control laws.

INTRODUCTION

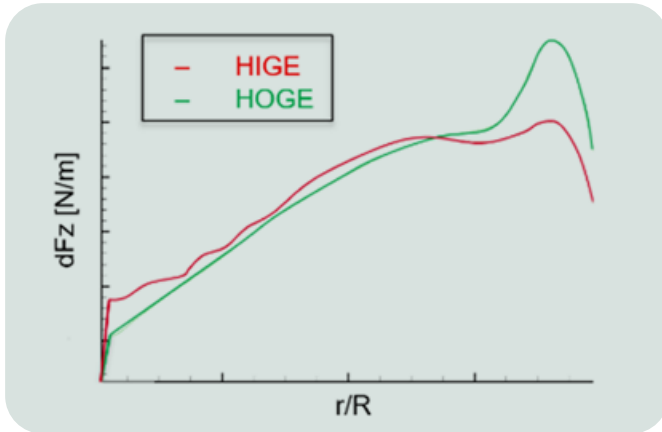
The incoming Next Generation Civil Tilt Rotor-Technology Demonstrator (NGCTR-TD) first flight has highlighted the need of including into the aeromechanic modelling approach the characteristic phenomenology exhibited by the side-by-side rotors configuration in ground effect. As highlighted by literature works, the effect of complex aerodynamic interactions between the rotor wakes, nacelles, fuselage, wing, and ground consistently alter the rotorcraft performances and dynamic response. In these conditions, the rotor blowdowns turn out to be trapped between fuselage, wing, nacelles, and, ground producing an “air cushion” that reduces the power required to hover, see [1][2]. On the other hand, such condition is usually characterized by reduced rotorcraft stability features, especially concerning the lateral directional axis. The macroscopic effect consists of a reduction of the rotorcraft “Roll Stiffness”, see [3]. Indeed, a perturbation of the aircraft roll attitude (and its consequent induced lateral velocity) alters the initial symmetry of the “air cushion”, [4]. The consequence is the production of differential starboard and port rotorcraft forces that result in a roll moment directed as the roll attitude changes.

In this regard, aeromechanic models capable of describing the complex aerodynamic interactions between the different components of the aircraft itself and the surrounding environment, i.e. ground, town walls, roofs etc. as well as heli decks become crucial for vendors to be owned. Indeed, the difficulty or impossibility to perform flight tests in such conditions with the possible damage of expensive prototypes requires the massive use of both offline and real time simulations with the pilot in the loop, [5]. In this context, the paper proposes a process aimed at the synthesis of analytical relations that are representative of the phenomenology described above, once being characterized by dedicated CFD analyses.

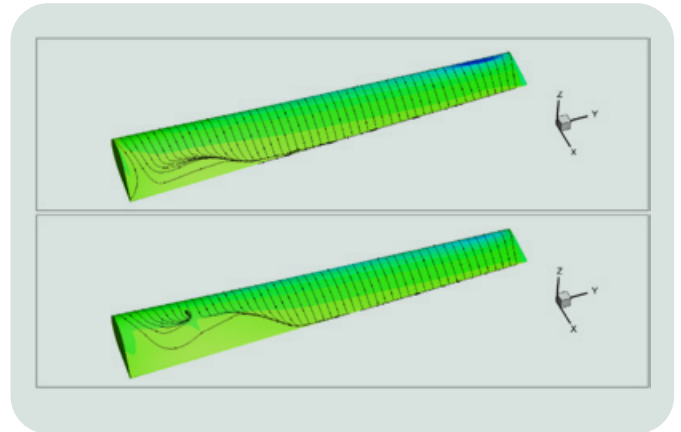
The effects of the proposed modelling approach are then assessed by considering the modification of steady rotorcraft attitude and pilot inputs in ground effect. The root locus obtained by varying the rotorcraft altitude from out to in ground effect conditions highlights the impact of ground proximity on the bare aircraft stability. Finally, effectiveness of the control laws synthesized out of ground effect in ground effect is assessed both in terms of closed loop system root locus features and of robustness by the means of disk-based stability margins.

HIGH FIDELITY AERODYNAMICS

In the framework of the aerodynamic evaluation of the prop-rotor Hovering In Ground Effect (HIGE) performances, dedicated 3D-CFD analyses have been carried out for an isolated rotor. The prop-rotor aerodynamic behaviour in terms of specific thrust distribution in and out of ground effect that is highlighted in Figure 1 reveals how the presence of the ground alters the rotor induction on the blade span.



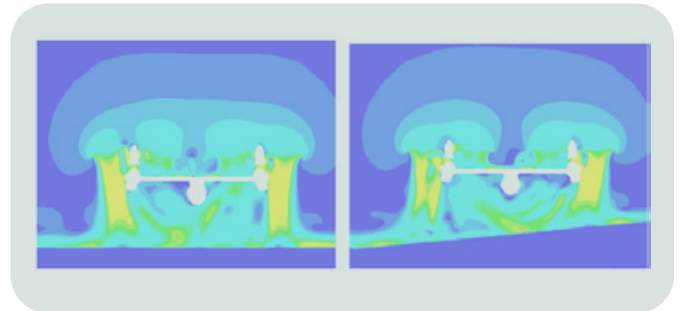
1 – Isolated rotor sectional blade force distribution as function of the nondimensional sectional spanwise positions (r/R)



2 – Pressure contour and wall shear stress lines on the suction side of an isolated rotor in hover out of ground effect (top) and in ground effect (bottom) at the same rotor pitch

Specifically: i) a reduction of the local Angle of Attack (AoA) on the outer blade stations, highlighted by a loss of thrust on the blade tip region; ii) increase of the inner blade sections AoA, due to the lower induction provided by the tip vortex (reduced downwash on the sections included by the tip vortex core helicoid). The latter contribution is usually the dominating one in standard helicopter configurations, as it provides beneficial effect of rotor performances in HIGE.

However, the characteristic high prop-rotor blade twist necessary to provide satisfying performances in both, airplane and VTOL mode, makes the former contribution the prevalent one. In these conditions, the inner rotor blade sections experience very high AoA in Hovering in of Ground Effect (HIGE) conditions being close to stall, see Figure 2. Overall, at constant collective deflection, the prop-rotor configuration shows slight diminished rotor thrust in HIGE with respect to HOGE conditions. In addition to the isolated prop-rotor behaviour, the effect of rotor wakes-airframe interactions in HIGE conditions has been characterized.



3 – Velocity magnitude contour of the in ground effect NGCTR-TD a) levelled (left), b) with a roll angle (right)

Concerning the longitudinal airframe response, a sensitivity analysis on the non-dimensional ground distance h/D , namely the ratio between symmetric rotor hub altitudes above ground and rotor diameter, has been carried out. The major outcome is the airframe download reduction, due to the “cushion” effect, see Figure 3 (a), whose characterization is done by considering the *airframe download coefficient* defined as by (1), being F_z the airframe download while T is the rotor thrust.

$$\frac{Ct_{A_{ige}}}{Ct_{A_{oge}}} = \frac{(F_z + T)_{ige}}{(F_z + T)_{oge}} \quad (1)$$

VERTIFLIGHT TECHNOLOGIES IN LEONARDO

Flight Condition Recognition, Simulation, System Design,
Tilt-Rotor technologies and System Integration

Remarkable increase in the airframe download coefficient has been found in ground effect, despite, as demonstrated in the former section, the NGCTR-TD rotor does not provide, as the conventional helicopter rotors do, any increase in thrust at a fixed pitch as far as the ground distance is decreasing. Thus, the download reduction is mainly attributed to the airframe.

A further finding is the presence of increased pitch up moment that is generated by the rotor wake development after having impacted the ground surface.

In order to characterize the lateral directional airframe aerodynamic response to ground surface in terms of Roll Stiffness, a sensitivity analysis has been performed at different aircraft roll settings considering constant symmetric non-dimensional ground distance h/D .

As shown in Figure 3(b), considering a positive attitude (wing-starboard down) the rotor wake closer to the ground turns out to be rapidly washed out towards the opposite side, which leads to an appreciable suction on the bottom of both the starboard wing and nacelle walls.

On the other hand, the port side experiences a completely different situation. Indeed, the rotor port wake and the one coming from the starboard side interact with each other, leading to a local over pressure. The difference on the integral F_z between the port and the starboard forces returns a roll moment, which leads the aircraft to further increase the roll attitude, thus providing positive value to the Roll Stiffness $\partial L/\partial \varphi$ (unstable behaviour).

AEROMECHANIC MODELLING

In this section the synthesis of analytic models based on the outcome of the former aerodynamic analyses is presented.

Rotor

In order to correlate the outcomes of isolated aeromechanic prop-rotor model with the high fidelity aerodynamic performance dataset, a user defined scheduling of inflow correction parameter has been defined, see [6]. This approach is based on the hypothesis of constant rotor power and allows to adjust the predicted rotor thrust by tuning the induced velocity with a coefficient, namely k . By recasting the constant power hypothesis between HIGE and HOGE conditions, using the inflow correction parameter to relate the induced velocity in and out of ground effect the ratio between thrusts reads:

$$T_{ige}/T_{oge} = 1 / \left[1 + k_1 \left(\frac{h}{d} \right) e^{-k_2 V_{gr}} \right] \quad (2)$$

In (2) V_{gr} is the horizontal rotor speed, k_1 and k_2 are coefficients accounting for the effect of rotor height over ground and rotor horizontal speed, respectively. The function $k_1(h/D)$ is obtained by imposing in (2) $V_{gr}=0$ and the ratio $T_{HIGE}/T_{HOGE}(h/D)$ as provided by CFD data, whereas k_2 is taken from literature outcomes, [4].

Airframe Lateral Axis

In order to model the lateral axis airframe aerodynamic response in ground effect, an approach similar to the one proposed by [4] has been chosen. Specifically, an additional rolling moment in ground effect has been implemented as follows

$$L\left(\frac{h}{D}, \phi, V_G\right) = \alpha \left[\hat{L}_0 + \hat{L}_1 \frac{h}{D} + \hat{L}_2 \frac{h^2}{D^2} + \hat{L}_3 \frac{h^3}{D^3} \right] \phi e^{-k_4 V_{gr}} \quad (5)$$

Airframe Longitudinal Axis

From the CFD aeroloads, breakdown force and moment contributions in HIGE conditions are available for each rotorcraft components, namely: wing, nacelles, fuselage and tail. The modelling approach is based on the scheduling of delta vertical forces ΔZ_i and pitching moments ΔM_i between CFD data and the outcomes of standard aeromechanic model implementation in HOGE as follows:

$$\Delta Z_i = [Z_{iCFD}(h_i/D) - Z_{iFL}(h_i/D)] \frac{C_t}{C_{tref}} e^{-k_3 V_{gr}} \quad (3)$$

$$\Delta M_i = [M_{iCFD}(h_i/D) - M_{iFL}(h_i/D)] \frac{C_t}{C_{tref}} e^{-k_3 V_{gr}} \quad (4)$$

In (3) e (4) the subscript i represents the i -th airframe component i.e. wing, nacelle, tail and fuselage. In order to widen the applicability of such corrections to different rotorcraft speeds and gross weights, the following two hypotheses are applied:

- The airframe download decays exponentially with the horizontal rotorcraft speed as by the constant k_3 (suggested by [4]);
- The airframe download correction is proportional to the ratio between rotor actual thrust and the reference one at which the CFD data have been obtained.

The polynomial shape function in (5) has been taken from [4] and scaled in order to match the symmetric NGCTR-TD rotors non dimensional height over ground at touch-down. The exponential decay coefficient k_4 in (5) is the same of that proposed by the literature reference, whereas α is such to provide the same value of Roll Stiffness predicted by CFD results in hover conditions at the considered h/D .

HIGE TRIM CONDITIONS AND BARE AIRCRAFT STABILITY

The effects of modelling HIGE conditions as proposed in the former section are inhere assessed in terms of:

- Rotorcraft attitudes and pilot inputs in steady conditions;
- Bare aircraft Linear Time Invariant (LTI) model root locus.

The following results only focus on HIGE conditions, being those the most impacting in terms of trim conditions and stability features modifications. As shown by previous studies (not inhere reported), a substantial weakening effect of the highlighted ground effect phenomenology is induced by the horizontal rotorcraft speed, due to the rotor wakes convection behind the rotorcraft.

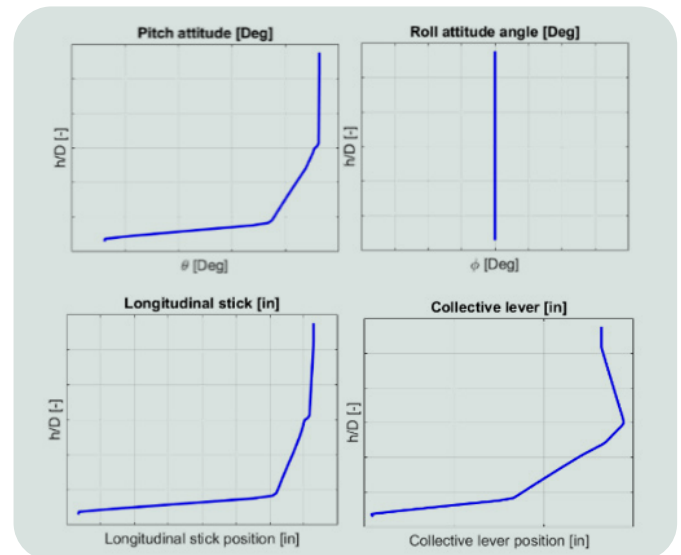
Trim conditions

As depicted in Figure 4, the rotorcraft pitch attitude decreases as the proximity to the ground increases, whereas the roll angle remains null due to the assumed null value of A/C center of gravity butt line.

For tiltrotor configurations, the effect of diminished pitch angle as closing the gap with the ground is known and mainly due to the rotor wake impingement on the tail, see [4].

In terms of collective pilot inputs, an initial increase as the distance from ground decreases is required to compensate for the rotor loss of thrust.

Then, below a certain h/D , the download reduction of the airframe in ground effect (cushion effect) is responsible for the diminished value of the collective that is required to balance the rotorcraft. Longitudinal lever position turns out to be less than in HOGE conditions (stick aft), due to the rotor wakes impingent on the tail via ground surface.



4 – Rotorcraft pitch and roll attitudes, longitudinal stick and collective lever position

Bare Rotorcraft Stability Assessment

The analyses are carried out by considering the eigenvalue problem associated to the reduced 8x8 state matrix of LTI (Linear Time Invariant) model, whose state vector is $x=[\varphi, \theta, u, v, w, p, q, r]$, being the elements roll and pitch attitude, linear velocities and angular body rates, respectively.

The mentioned LTI model is obtained by a proper model reduction (matched DC gain method, higher order dynamics residualization) of the full order model considering all the states describing the dynamics of the vehicle, see [6].

The assignment of mode shape to each eigenvalues is based on the Modal Participation Factor (MPF) computation, see [7]. The root locus changes from HOGE to HIGE conditions accounting for all the ground effect contributions as defined above are highlighted in Figure 5. Changes with respect to HOGE are substantial since all system poles are affected by the presence of ground.

Specifically, it can be noticed that:

- The longitudinal dynamics is only slightly affected by the ground effect. Specifically, the phugoid mode is stabilized and increases in frequency as h/D decreases. Moreover, heave and pitch subsidence couple into the short period whose frequency increases as h/D decreases;

VERTIFLIGHT TECHNOLOGIES IN LEONARDO

Flight Condition Recognition, Simulation, System Design,
Tilt-Rotor technologies and System Integration

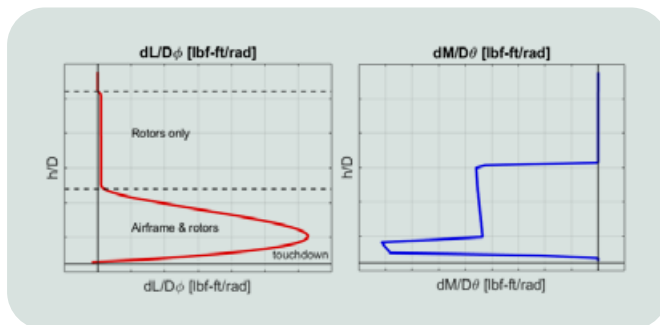
- The lateral-directional axis is the most affected by the ground proximity. Specifically, the Dutch roll shows substantial change of frequency and damping whose characteristics are function of the different value of h/D . The behavior of aperiodic modes is instead more linear, showing from HOGE increasing frequency up to reaching a maximum value for a given h/D followed by a frequency reduction till to the touch-down.

A further assessment about the previously discussed bare A/C modes frequency and damping alteration due to ground effect is depicted in Figure 6. The contributions breakdown shows the effect of:

- only lateral;
- only longitudinal;
- only rotor thrusts;
- all corrections applied.

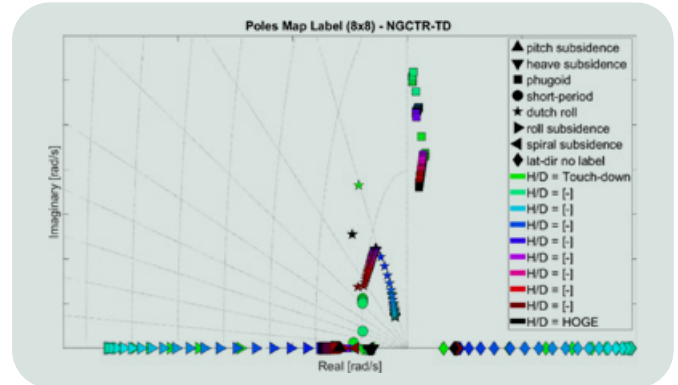
This confirms that the biggest contribution to the stability features modifications comes from the lateral dynamics correction.

Observing the roll subsidence and generic aperiodic lateral-directional mode frequency trend with the h/D the shape of L_ϕ derivative, shown in Figure 7 (a), can be easily recognized. The longitudinal dynamics correction affects mostly the phugoid mode: its frequency and damping variation with h/D recall the M_θ derivative, see Figure 7 (b), while the rotors thrust correction implies mainly a Dutch-roll mode damping reduction as h/D decreases toward the touchdown. This suggests that L_ϕ and M_θ derivatives are responsible for the most significant rotorcraft stability modifications in ground effect conditions.

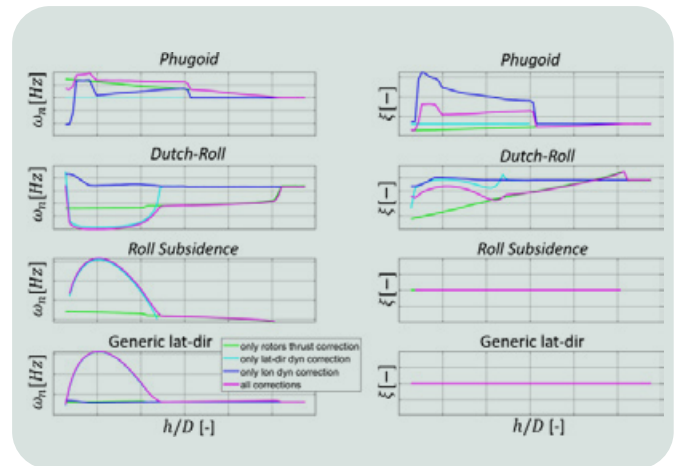


7-a) On the left L_ϕ
b) On the right M_θ ; derivatives at hover

Then, different control laws configurations are applied and the augmented A/C stability is assessed for each one, in terms of natural frequency and damping characteristics of the aperiodic lateral directional unstable eigenvalue. Finally, the robustness of CLAWs designed in HOGE, with respect to the model uncertainties introduced by the HIGE conditions, is assessed by the means of stability margins analysis through the disk-based approach, [8].



5-NGCTR-TD Root locus, of 8x8 state matrix from HOGE (black) to HIGE, (green is the wheel touchdown)



6-Ground effect mostly affected bare A/C modes frequency and damping trends as function of h/D , comparing each considered modelling configuration

AUGMENTED AIRCRAFT STABILITY ASSESSMENT

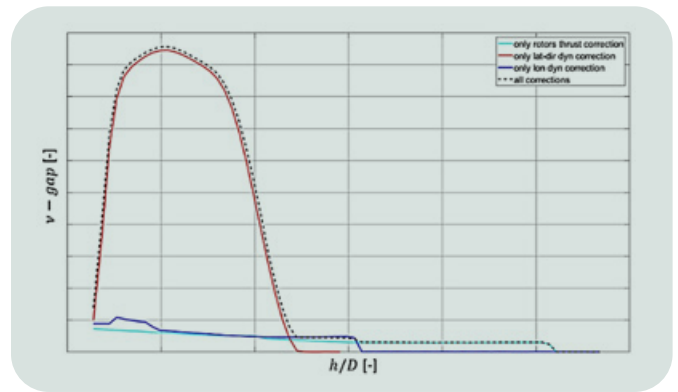
This section discusses the dynamic stability of the NGCTR-TD when the flight control system (FCS) loop closure is applied to the linearized bare A/C dynamics in hovering, at different height from ground. The section is organized as follows: first, an *a-priori* evaluation of how the alteration of reference HOGE model, due to the ground effect, will impact the closed-loop performance, before applying the actual CLAWs, is performed applying the v-gap metric, see [8].

The AyraDB Benchmarking Backend

The baseline Control Laws (CLAWs) design and synthesis is performed within a subset of HOGE Linear Time Invariant models take as reference. As a first instance, the CLAWs parameters scheduling as a function of the height from ground was not deemed necessary for basic control functions. Therefore, the effect of the ground is managed by the control system as a bare A/C model uncertainty, with respect to which the control system robustness has to be verified.

From this point of view, it is useful to carry out a preliminary verification by using the v -gap metric. The metric quantifies the distance between two dynamic systems in closed loop, without considering any control system. In the present case the dynamic systems are represented by the bare aircraft linear time invariant model (A/C LTI) in HOGE and each HIGE model at different h/D . The metric values satisfy $0 \leq v\text{-gap} \leq 1$. Values close to 0 imply that any controller stabilizing HOGE model also stabilizes the HIGE one with similar closed-loop gains, it runs viceversa if v -gap tends to 1.

In Figure 8 the v -gap worst-case for each h/D (peak value along frequency) is shown, representing the worst-case drop in closed-loop performance. The L_ϕ derivative Figure 7 (a) trend can be found when observing the v -gap as a function of h/D in cases with only lateral dynamics correction and all corrections applied, with a peak close to one (maximum expected closed-loop performance drop respect to HOGE) at the same h/D where the A/C rolling moment correction due to ground effect is maximum. The v -gap considering only longitudinal dynamics and rotors thrust correction remains below 0.1, confirming the very low alteration of closed-loop performance respect to HOGE; similarly for the longitudinal dynamics correction cases the v -gap behaviour recall the M_ϕ derivative, see Figure 7 (b).



8- v -gap metric between HOGE bare A/C model and HIGE as function of h/D , for each considered ground effect modelling

Closed-loop A/C Dynamic Stability Analysis

The complementary sensitivity transfer function of a negative feedback loop $F(s)$, namely the closed loop system transfer functions, is defined from the considered LTI bare aircraft model $G(s)$ and controller $C(s)$ by the following equation:

$$F(s) = G(s)C(s)[I + G(s)C(s)]^{-1} \quad (6)$$

In order to get closed loop stability features the $F(s)$ transfer function is converted into state-space form and state matrix eigenvalues are analysed, using the Modal Participation Factor technique [7], to identify the modes shape.

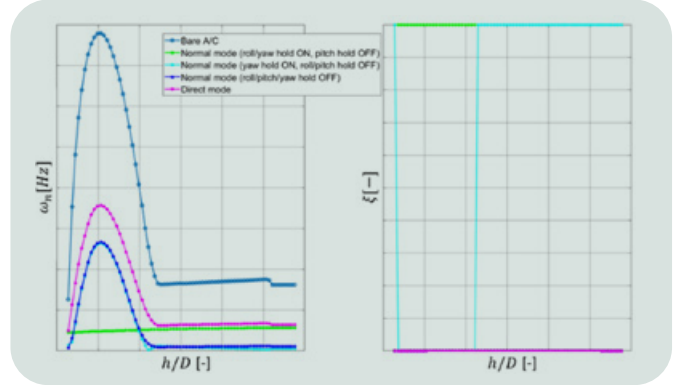
The plant transfer function $G(s)$ herein considered concerns the LTI bare aircraft model from HOGE to HIGE conditions whereas the following four different FCS configurations are considered for the present analysis, namely:

- Direct mode: implementing a basic Stability Augmentation System (SAS) on the three axis angular rates with only damping effect (no integral terms);
- Normal mode configured Hands-On/Feet-On: together with the SAS also the attitude control loops are active, but when pilot hands and feet are acting on commands the attitude hold function on roll/pitch/yaw angle is disabled;
- Normal mode configured Hands-On/Feet-Off: respect to the previous the pilot feet are off the pedals, hence the attitude hold function on yaw angle is enabled, roll/pitch attitude hold function is disabled;
- Normal mode configured Hands-On longitudinal/ Hands-Off lateral/Feet-Off: respect to the previous the pilot hands are off the lateral command, hence the attitude hold function on roll and yaw angle are enabled, pitch attitude hold function is disabled.

From the previous FCS configurations, the level of control augmentation is progressively incremented. An easier way to capture the effect of the described progressive increment of control law actions on the closed loop system, is the migration of the generic lateral-directional aperiodic mode on the Gauss plane as a function of h/D , changing the FCS setting, is presented in Figure 9.

Observing the damping subplot, the lower value (-1) indicates instability, while the upper (+1) the stability. Hence, the mode is stabilized for all the h/D only when the CLAWs are set to *Normal mode* with roll/yaw attitude hold On.

Conversely, it is stable, except in a certain h/D region, for the Normal mode with yaw attitude hold On (roll hold Off) and always unstable in case of Normal mode with roll and yaw attitude hold disabled and Direct mode. From the frequency subplot of Figure 9 it is possible to recognize again the same trend of the L_φ derivative along h/D (Figure 9).



9–Generic lateral-directional aperiodic mode frequency and damping as a function of h/D

Stability Margins Analysis

In the present work it was preferred to adopt the disk-based stability margins method instead of the canonical *loop at time* approach since it considers a concurrent perturbation on both gain and phase and on all the channels of the control system at the same time. Hence it provides a stronger guarantee of closed-loop stability than the classical gain and phase margins. For each combination of bare A/C hovering model G and controller C corresponding to considered CLAWs settings, the evaluation of disk-based stability margins with changing height from ground was performed by defining the complementary sensitivity function with respect to the process output (sensors) as:

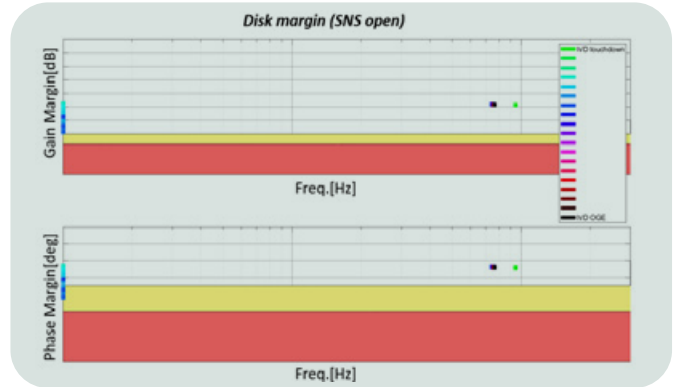
$$F_y(s) = G(s)C(s)[I + G(s)C(s)]^{-1} \quad (7)$$

and the complementary sensitivity function respect to the process input (commands) as:

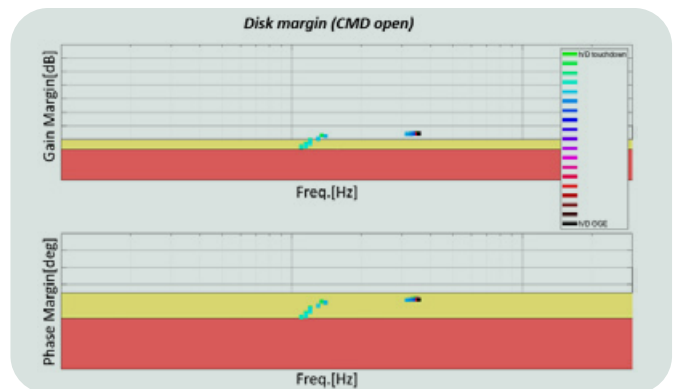
$$F_u(s) = C(s)G(s)[I + C(s)G(s)]^{-1} \quad (8)$$

The MIMO control system open-loop transfer functions on which disk-based margins are computed are: i) sensors opening (SNS) $L(s)=G(s)C(s)$ and commands opening (CMD) $L(s)=C(s)G(s)$.

As depicted in Figure 9, the closed loop system is stable at any h/D when *Normal mode configured Hands-On longitudinal/ Hands-Off lateral/Feet-Off CLAWs* configuration is adopted. In this conditions the disk-based gain/phase margin analysis is meaningful, since it provides phase and gain margins of a stable closed loop system. Figure 10 and Figure 11 depict the minimum disk-based gain and phase margins (in sensors and commands opening cases respectively) as function of the frequency at which the minimum occurs.



10–Minimum disk-based gain/phase margins (sensors opening) as function of frequency, hovering condition changing h/D



11–Minimum disk-based gain/phase margins (commands opening) as function of frequency, hovering condition changing h/D

The coloured regions indicate company internal gain and phase margin requirements for the FCS design: white is the desired positioning, yellow the adequate and red the non-compliance. Therefore, the augmented A/C in hovering is compliant with stability margins design requirements whatever is the height from ground.

The result assesses the robustness of the controller design on the HOGE model to the ground effect disturbances on the bare A/C dynamics. However, it is evident a reduction of stability margin in HIGE with respect to the nominal HOGE condition, by a consistent amount: at the worst h/D , for the command opening case, both gain and phase margins result close to fall in the not compliance region.

CONCLUSIONS

The paper dealt with the synthesis and assessment of a ground effect model for tiltrotor-like configurations suitable for real time pilot in the loop analyses. Dedicated CFD analyses, carried out on the NGCTR-TD tiltrotor configurations have highlighted the following phenomenology related to the interactions with the ground surface:

- Prop-rotors providing diminished thrust when entering in ground effect conditions due to portions of stalled rotor blades close to the root;
- Rotors wake impingement on tail via ground altering the longitudinal set of forces and moments;
- Rotors wake impingement on the fuselage belly and wings via ground altering the aerodynamic lateral forces and moments in presence of roll attitude.

On the basis of these outcomes analytic models have been derived and implemented in the aeromechanic model to account for the mentioned phenomenology. Then, the assessment of the bare aircraft trim and dynamic stability in ground effect shown the following main outcomes:

- The rotorcraft trim attitudes and pilot inputs are consistently affected by the ground surface. Specifically, pitch attitude and longitudinal stick positions monotonically decrease (pitch down and stick aft) when entering in ground effect due to the rotor-wake impingement on the tail. The beneficial effect of the reduced wing download in ground effect is appreciable on the collective lever position only after a preliminary phase, at higher h/D , where the rotor diminished thrust plays the major role.
- Longitudinal stability is affected by the presence of ground showing a slight stabilizing effect on the phugoid mode.

- Lateral stability is strongly affected by the presence of ground. The effect is due to the positive feedback induced by the roll angle on the rolling moment produced by the rotors wake impingement on the rotorcraft belly and wings. Similar, although weaker, is the effect induced by the rotor diminished thrust in ground effect. All the lateral poles are consistently affected, the Dutch roll showing diminished damping and natural frequency as well as the aperiodic modes showing increased natural frequency values.

Finally, the impact of the modelled ground effect on the control laws synthesis and the augmented NGCTR-TD dynamics have been assessed. The most critical bare A/C mode of IGE hovering dynamics is the unstable generic aperiodic lateral-directional one (modal participation on ϕ , p , v , r states in decreasing order). The basic FCS configuration with angular rates dampers only (SAS) is not able to obtain its stabilization: it was strictly needed to add also attitude control loops and enable both bank and heading hold functions to meet the ADS-33 Lv1 dynamic stability requirements. The stability margins of the designed control loop for the HOGE condition is assessed by means of disk-based methodology: the compliance with gain/phase margins design requirements is achieved for each height from ground, demonstrating an adequate robustness of the controller to the ground effect disturbances, without the introduction of CLAWs parameters scheduling as a function of the height from ground. Nevertheless, a significant reduction of stability margins in HIGE respect to the nominal HOGE condition was experienced: at the worst h/D , both gain and phase margins resulted close to fall in the not compliance stability margins region, proving the strong ground effect impact on tilt-rotor's hovering lateral-directional dynamics.

Concluding, the new process adopted (considering an optimized and integrated approach between different topics) has permitted to improve the model accuracy, with possibility not only to have a smart approach for pilot-in-the-loop simulations, but also to investigate design choices to strengthen the safety of flight for novel platform.

VERTIFLIGHT TECHNOLOGIES IN LEONARDO

Flight Condition Recognition, Simulation, System Design,
Tilt-Rotor technologies and System Integration

REFERENCES

- [1] Polak, D. & Rehm, W. & George, A. (2000). Effects of an Image Plane on the Tiltrotor Fountain Flow. Journal of The American Helicopter Society - J AMER HELICOPTER SOC. 45. 10.4050/JAHS.45.90.
- [2] Radhakrishnan, A.M. An Experimental Investigation of Ground Effect on a Quad Tilt Rotor in Hover. Journal of the American Helicopter Society. 60, 012002 (2015).
- [3] Etkin, B. (1959). Dynamics of Flight: Stability and Control, Wiley
- [4] Rosenstein, H., Mcveigh, M. A., Mollenkof, P. A., V/STOL tilt rotor aircraft study mathematical model for a real time simulation of a tilt rotor aircraft , (Boeing Vertol Model 222), volume 8, September 2, 2013, April 1, 1973, Report/Patent Number D222-10061-1-VOL-8 NASA-CR-114601
- [5] <https://www.easa.europa.eu/en/research-projects/rocs>.
- [6] <http://www.flightlab.com>.
- [7] T. Femi and S.J. Mija – Modelling of Hovering Helicopter and its Stability analysis using Participation Factor – IFAC PapersOnLine 51-1 (2018) 504-511.
- [8] Cantoni, M. and Vinnicombe, G., Quantifying uncertainty and robust performance using the v-gap metric. AIAA Guidance, Navigation and Control Conference, Portland, USA, pages 1624–1630, 1999.

Coupled Torsional Dynamics and Gear Contact Model to Predict Tiltrotor Drive System Loads

Ahmad M. Haidar, Nathaniel Albuck

Leonardo – Helicopters Division

The tiltrotor drive system is a complex and coupled system with different torsional dynamics compared to conventional helicopters. It is designed to guarantee safety and reliability and tested for the effects of its dynamics and loads on component sizing. Components such as the final reduction stage in the rotor gearbox are most impacted by such dynamics and must withstand all peak loads due to novel control strategies and torsional dynamics. In this paper, a gear contact analysis model is coupled with a validated torsional dynamics model of a tiltrotor interconnected drive system. The coupled model predicts component-level loads in the interconnected drive system originating from its torsional dynamic behavior. A dynamic overload factor relating the peak dynamic and static loads is analytically assessed, and it is shown to exceed conventional predictions in the case of an asymmetrically loaded interconnected drive system.

INTRODUCTION

The drive systems of tiltrotors and multi-rotor powered lift aircraft with mechanical interconnects exhibit unique torsional dynamic behavior [1]. The dynamic interactions in the drive system result in component level loads that must be determined from either a costly test program and/or through development of novel analytical methods that could reduce the cost of testing and validation. This paper describes the development of a framework that can be used to analyze component level design loads in the drive system originating from this unique torsional dynamic behavior of interconnected drive systems. The focus of this paper is the final reduction planetary stage of a tiltrotor drive system similar to the AW609 tiltrotor aircraft (see Figure 1). Previously, Haidar et al. in [2] presented the drive train torsional stability analysis and certification test campaign for the AW609 tiltrotor. There, the analytical predictions were correlated with flight test measurements thus validating the model. The AW609 is a nine-passenger civil tiltrotor designed for all-weather operations at flight speeds ranging from hover to 275 kts. The flight envelope includes altitudes up to 25,000 ft (7,620 m).

This is then followed by a test program that is used to further validate the safety of the design. While the aircraft and sub-system level tests validate the functionality, structural integrity, performance, and serviceability, the measurement of loads on individual gear stages is generally omitted. Whereas in component or subassembly level tests, the interactions resulting from unique torsional dynamics of the drivetrain are not included.



1 – AW609 tiltrotor aircraft in flight

VERTIFLIGHT TECHNOLOGIES IN LEONARDO

Flight Condition Recognition, Simulation, System Design,
Tilt-Rotor technologies and System Integration

Therefore, a method for accurately predicting the dynamic loads at component level in tiltrotors is required to (a) capture peak loads and system excitations during asymmetric maneuvers for structural design and sizing, and (b) optimize the phasing (angular spacing) of the planet gears for uniform load sharing between all planet gears. Investigation of planet load sharing and phasing is an active area of research, especially for jet engines and wind turbine power gearboxes (see [3] [4] [5] and [6]).

Work done by Beinstingel et. al in [7] establishes a 13 DOF torsional dynamics model of a test setup that includes motor and generator (load) and couples the planetary stage torsional dynamics with a larger system dynamics model. These systems, however, are characterized by a single (or multiple) rotors on a single axis. This is the key difference with tiltrotor (or multicopter) drive system architecture; the tiltrotor drive system is a multiple input (engine torque), and multiple output (rotor torque) system should impacts how individual dynamic components are designed. The tiltrotor drive system planetary stage, like most helicopter planetary gearboxes, is constituted by spur gears. The input is at the sun gear, and the output is at the carrier which is splined to the rotor mast. The ring gear is fixed to the gearbox housing. There are multiple planets in the planetary stage, and the usual design practice is to assume equal load distribution for all planet gears.

This assumption will not be true if the planet gear phasing is offset or there are assembly or manufacturing deviations. Furthermore, the effect of input and output torque fluctuations that arise from asymmetric maneuvers must be addressed. This work aims to establish the overload factor that originates from the dynamic load distribution analysis, and an optimal angular phasing of the planetary gear meshes to suppress tonal noise from the gearbox while ensuring a uniform load sharing between the planets.

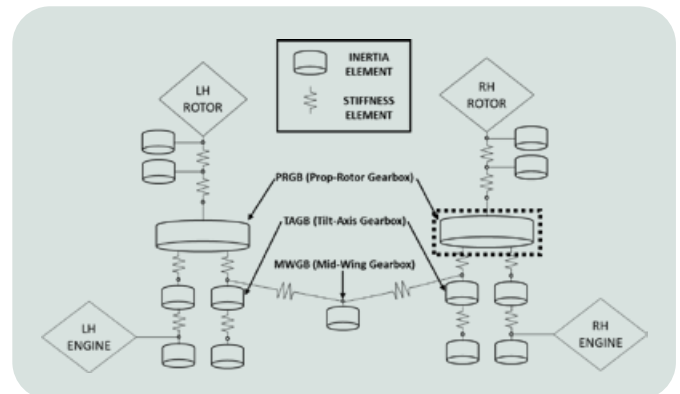
MODEL DEVELOPMENT

A drivetrain torsional dynamics model is extended with a detailed dynamic load distribution and contact analysis model for the planetary gear stage. The dynamics models are presented in this section, and the coupling scheme between them is detailed.

Tiltrotor Drive Train Model

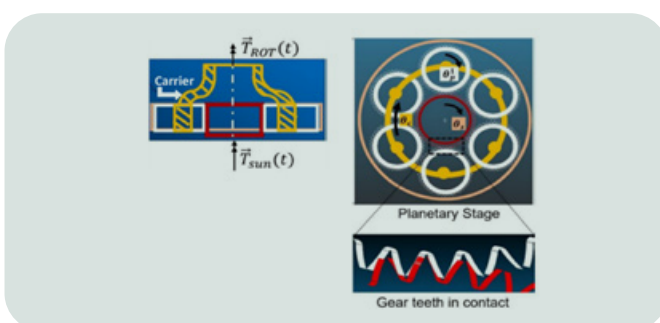
The drive train dynamics model, developed in [2], is a system of lumped mass inertial elements connected by stiffness elements (torsional springs). Each element models the physical properties of each stage of the tiltrotor drive system from the engine input to the rotor, and the interactions between each reduction stage.

The original intent for this model was to demonstrate the dynamic stability within the system, however the model is valuable also for its ability to simulate the dynamic loading to each subsystem. The basic drive system elements and cross-coupling of the two rotor torques via an inter-connecting shaft system are shown in Figure 2.



2-Lumped tiltrotor drive train model

Planetary Gear Train Model



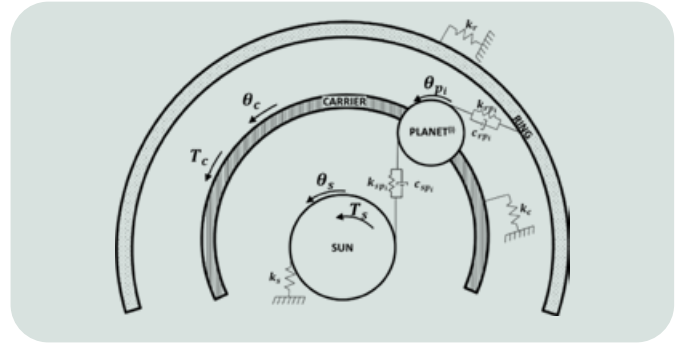
3-Details of the Planetary gear stage of the PRGB node

A detailed model is used for the planetary stage in the prop-rotor gearbox (PRGB) node of the lumped parameter torsional dynamics model. The gearbox consists of 3 reduction stages of which the final stage is a planetary gear train (PGT). An overview of the planetary gear train is provided in Figure 3 with the state variables, θ , for each of the dynamic components in the PGT stage. At the center of the planetary gear system is an external spur gear known as the “sun gear”. The sun gear interacts with several spur gears, anywhere from 3 to 8, spaced along its circumference, and these are referred to as “planet gears”.

These planet gears rotate around the sun gear while mounted to a carrier which connects them to one another. The planet gears simultaneously mesh with an internal gear which is concentric with the sun gear, called the ring gear. The power transmission through these systems can vary depending on which of these components is fixed in place. In the system explored in this study, the ring gear is fixed making the sun and carrier the power input and output, respectively.

The PGT dynamics model is based on the mathematical system of equations described by Öztürk in [8] and adapted by Albuck et al. in [9]. A schematic of the model is presented in Figure 4. Like the dynamics model for the larger tiltrotor drive train, the components of the PGT are modeled as lumped masses.

Parallel springs and dampers are used to model the tooth interactions between components along their lines of action. These elements are nonlinear, time-varying, and highly sensitive to gear profile modifications and misalignments. Thus, there is a need for a gear mesh contact model.

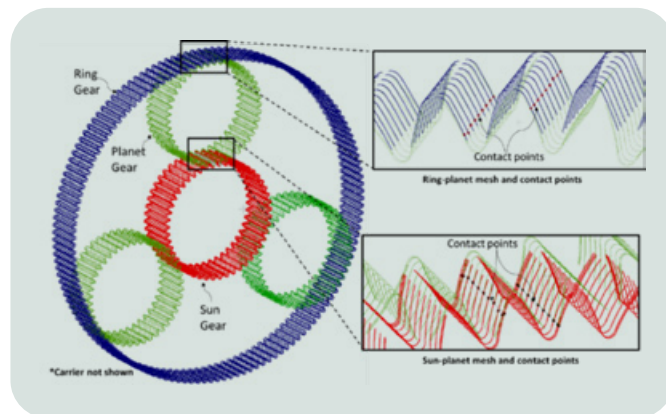


4–Diagram of planetary gear train model

Gear Mesh Contact Model

An accurate gear tooth contact analysis (TCA) that can interface with the dynamics model is critical to understand the loads on the gear teeth. An in-house gear contact analysis tool is developed with the capability to (1) generate or import the precise microgeometry of the gear teeth, (2) position the gears in space, (3) apply a torque load, and (4) carry out the gear contact analysis.

The primary function of the tool is to predict load distribution on multiple gear teeth in contact using a strain energy-based formulation. Profile/lead modifications, initial separation of the gear teeth surfaces, errors, and misalignments are accounted for. The approach used for calculating load distribution is described in [10] and [11]. It is possible to analyze both internal and external gear meshes for spur and helical gears with misalignments and/or profile modification.



5–Gear surface point clouds and contact points determined from the nearest neighbor search algorithm

In this work, the macro-and micro-geometry, with profile and lead modifications, are generated from production drawing data. Once the load distribution is calculated, closed form formulae are used to calculate the deflection of the gear teeth, such as described in [12]-[14]. The gear surface point cloud generated by the in-house tool using the inputs from the production drawing is shown in Figure 5. Complete 3D geometry of the gear profiles along with the tip relief and end reliefs is generated. Alternatively, a point cloud can be imported for further processing and analysis. The tool can generate gear teeth accurately and position them into contact to represent actual assembly. Therefore, different mesh phasing configurations can be simulated, and it is possible to implement the planetary gear kinematics in the tool and understand how the contact conditions evolve at each interface over a period of gear meshing, t_{mesh} .

In Figure 5, all planet gear meshes are in phase, however depending on the number of teeth, sequential and counter phasing can be achieved for planetary gear trains with 4 or 6 planets. Sequential or counter phasing of the planets results in a phase difference between time-varying mesh stiffness functions of each planet gear interfaces ([15]). This phase difference affects the dynamic response of the PGT, and its effects on the dynamic overload factor is explored in this paper. After the gear geometry is generated, the contact points are determined using a fast, nearest neighbor search algorithm.

VERTIFLIGHT TECHNOLOGIES IN LEONARDO

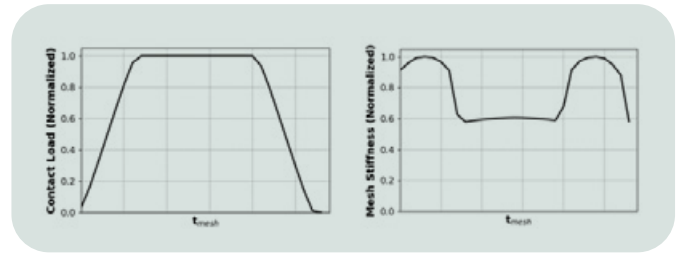
Flight Condition Recognition, Simulation, System Design,
Tilt-Rotor technologies and System Integration

This approach has been successfully implemented in past works to determine contact points such as in [16] and allows for the use of dense point clouds without any compromise in speed. This method of contact point determination is robust when considering gears that may be misaligned or displaced from their original position due to torsional vibrations.

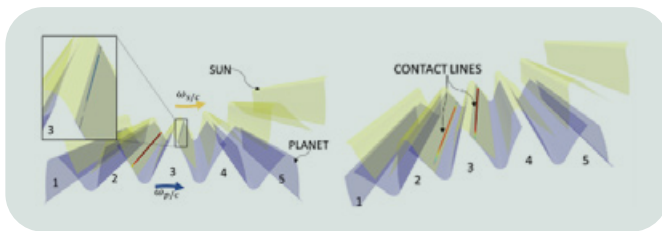
Next, the contact simulation is performed for one complete mesh cycle of a single tooth at different instances of time to determine how the load share of a single tooth evolves as it goes through the mesh cycle.

For a gear with n number of teeth, the mesh cycle characteristics will be repeated n times in a single rotation of the gear. Therefore, the excitations in the system caused by changes in the contact conditions happen at very high orders of the input speed.

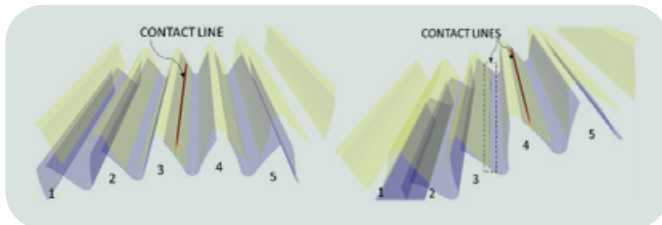
For the planetary gear set analyzed in this work, the gears have spur teeth with a linear tip relief and parabolic end relief. A sample of the results from the mesh cycle contact simulation are plotted in Figure 6. Here, the periods of single tooth contact are shown in terms of normalized contact load and mesh stiffness.



6-Periodic load and mesh stiffness of a single planet tooth



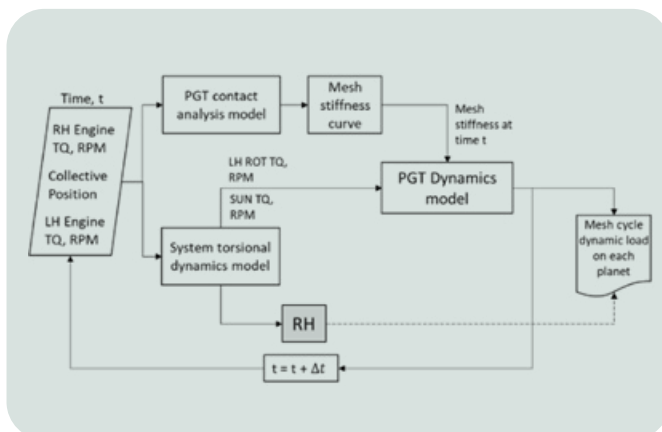
7-Contact stress on Tooth #3 at start of contact and with two teeth coming into contact



8-Contact stress on Tooth #3 at single tooth contact (100% of load) and at end of contact

The load peaks when the single tooth is carrying the entire mesh load, while the stiffness drops to 60% of its maximum value as the contact progresses. To demonstrate the mesh cycle, contact stress contours on the gear teeth are visualized in Figure 7 and Figure 8 as two gears rotate and Tooth #3 goes through its mesh cycle.

The Figures provide information on the number of teeth in contact as well as the relative length and thickness of the contact lines. The contact stress intensity is shown on a color scale ranging from blue to red. Note that due to the end reliefs on the gear face width, the contact stress intensity decreases towards the end of the gear face.



9-Scheme to evaluate dynamic mesh loads in tiltrotor drive system

Coupled Model

The individual, detailed models are coupled in a framework that is presented in Figure 9. To arrive to the component-level mesh loads, the tiltrotor drive train torsional dynamics model is first simulated, and the PRGB loads are determined. The PRGB loads are then applied at the sun gear and planetary carrier in the planetary gear train dynamics model.

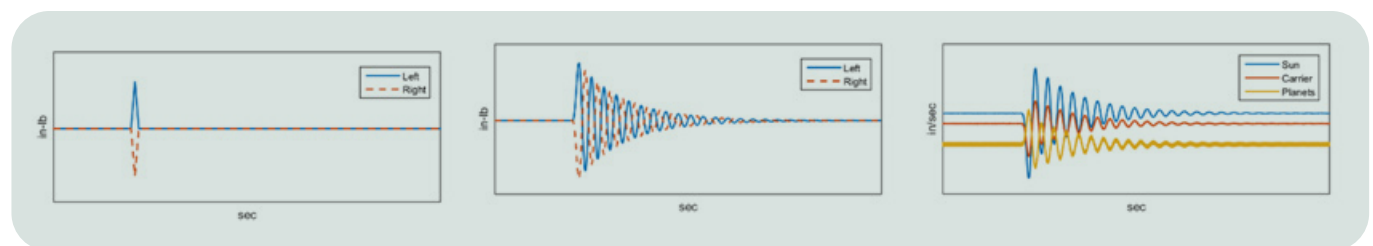
The time-varying mesh stiffnesses of the bodies in contact, which were determined using the gear mesh contact analysis model, is applied in the PGT dynamics model. The simulations of the coupled system are performed via a 4th order Runge-Kutta numerical integration algorithm.

RESULTS

The results of the analysis using the described models are presented in this section. Results from simulations of the coupled torsional and gear contact dynamics are presented for three cases with different gear phasing configurations: counter phased, sequentially phased, and in-phase gears.

The phasing of the planet gears affects when the mesh stiffness cycle (see Figure 6) begins for each gear relative to one another. With any offset in phasing, the gears come into contact at the interfaces either in unison or at a time offset. Importantly, this affects the instantaneous load sharing between the gears and the dynamics of the gear train.

For the simulations, a drive train load case was selected to highlight the asymmetric loading condition that can arise in interconnected drive trains in multi-rotor aircraft such as tiltrotors. In this case, the left and right rotors are excited by an equal pulse load that is 180 degrees out of phase across the rotors as shown in Figure 10.



10 – Rotor torque input
(asymmetric pulse)

11 – Drive train response
at rotor

12 – Gear response
at subcomponents

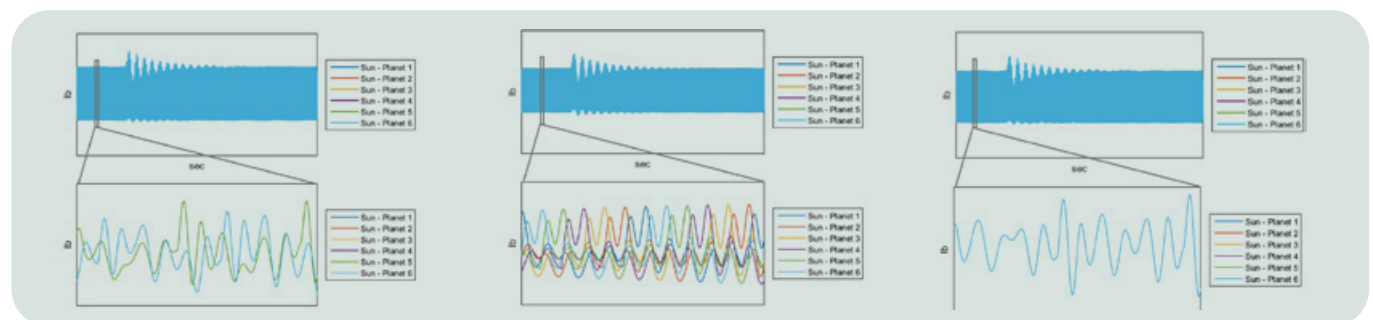
The drive train torsional dynamics model predicts the torsional response of the drive train as shown in Figure 11. The asymmetric pulse is effective at exciting torsional dynamics in the drive train. The pulse induces drive train oscillations that decay, and the coupled model then predicts the response of the planetary gearbox as shown in Figure 12.

With gear torsional responses (displacements) and mesh stiffnesses known, the interface mesh loads are calculated. The sun/planet interfaces are presented in Figure 13, Figure 14, and Figure 15 for counter phased, sequentially phased, and in-phase gears, respectively. The figures contain an enlarged section of the steady-state response to showcase the high frequency content of the signal. Note that the responses of some gears are not visible since they are identical in some cases when sharing a phasing.

The frequency content of the predicted mesh load is analyzed, and the loads at the gear harmonics are presented in Figure 16. The configuration – specifically the phasing of the gears – had an impact on the predicted loads in this high frequency domain. The in-phase gear configuration had dramatically reduced loads in the 1st harmonic with comparable loads on the remaining harmonics. Mitigating loads at these high frequency harmonics can prolong component life, increase safety, and reduce noise.

Finally, an overload factor is presented for all gear phase configurations in Figure 17.

This factor is calculated by dividing the maximum dynamic mesh load by the static load, and this is done at each gear interface. In steady state conditions, the overload factor is constant, but increases under the asymmetric torque loading.



13 – Mesh load at sun/planet interface
with counter phased gears

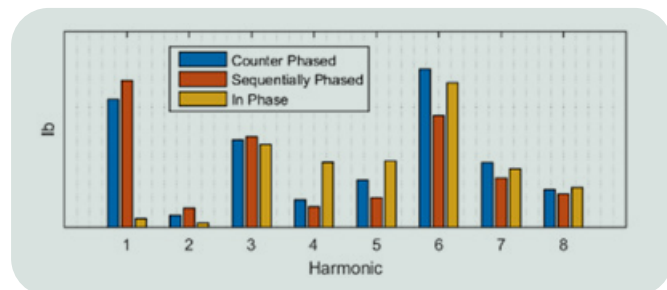
14 – Mesh load at sun/planet interface
with sequentially phased gears

15 – Mesh load at sun/planet interface
with in-phase gears

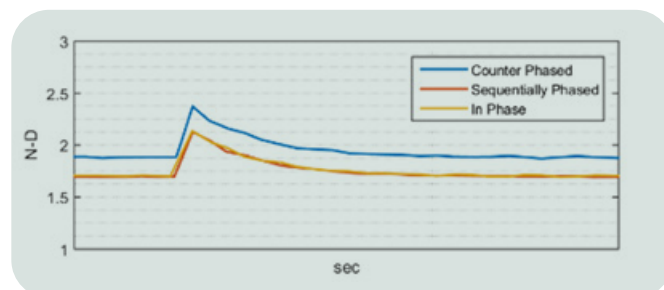
VERTIFLIGHT TECHNOLOGIES IN LEONARDO

Flight Condition Recognition, Simulation, System Design,
Tilt-Rotor technologies and System Integration

The torsional dynamics of the drive train and the asymmetric loading evidently contribute to the mesh load at the interfaces.



16–Mesh load harmonics



17–Overload factors

CONCLUSIONS

A coupled planetary gear train and tiltrotor drive system dynamics model was developed with accurate gear mesh stiffness from a contact analysis model. The torsional dynamics interactions between an interconnected multi-rotor drive train and its subcomponents were analytically evaluated for the first time.

Planetary gear stages with counter phased, sequentially phased, and in-phase planet gears were studied.

Subcomponent peak dynamic loads were determined in the case where the rotors are subject to asymmetric torque such as in maneuvers with differential collective pitch or gust.

Results demonstrate a dynamic load factor 2.3 times the design load. This load amplification must be considered when designing gears for static strength. A guidance can be established on phasing relationships of the planets to reduce the dynamic load factor and gear noise.

Ahmad M. Haidar: ahmad.haidar@leonardocompany.us

REFERENCES

- [1] P.R. Darmstadt, S. Pathak, E. Chen, A. Arkebauer, A. Beiderman, C. Dillard and M.P. Mistry, “Distributed Electric Propulsion and Flight Control Concept to Meet EASA SC-VTOL-01 10-9 Catastrophic Failure Criteria,” in Vertical Flight Society’s 77th Annual Forum & Technology Display, Virtual, 2021.
- [2] A.M. Haidar, L. Belluomini and A. A. Trezzini, “AW609 Civil Tiltrotor Drive Train Torsional Stability Analysis and Certification Test Campaign,” in The Vertical Flight Society’s 77th Annual Forum and Technology Display, Virtual, 2021.
- [3] Y. Guo and J. Keller, “Validation of a Generalized Formulation for Load-Sharing Behavior in Epicyclic Gears for Wind Turbines: Preprint,” National Renewable Energy Lab. (NREL), Golden, CO (United States), 2020.
- [4] Y. Guo, J. Keller and W. LaCava, “Combined effects of gravity, bending moment, bearing clearance, and input torque on wind turbine planetary gear load sharing,” National Renewable Energy Lab.(NREL), Golden, CO (United States), 2012.
- [5] L. Ryali, A. Verma, I. Hong, D. Talbot and F. & Zhu, “Experimental and theoretical investigation of quasi-static system level behavior of planetary gear sets,” Journal of Mechanical Design, vol. 143, no. 10, 2021.
- [6] C. Wang and R.G. Parker, “Nonlinear dynamics of lumped-parameter planetary gears with general mesh phasing,” Journal of Sound and Vibration, vol. 523, 202.
- [7] A. Beinstingel, R.G. Parker and S. Marburg, “Experimental measurement and numerical computation of parametric instabilities in a planetary gearbox,” Journal of Sound and Vibration, vol. 536, 2022.
- [8] V.Y. Öztürk, A Parametric study on planetary gear dynamics (PhD Dissertation), Ankara, Turkey: Middle East Technical University, 2018.

- [9] N. Albuck, A.M. Haidar, and T.D. Mathur, “Development of a coupled torsional dynamics and gear contact model to predict peak loads in a tiltrotor drive system,” in The Vertical Flight Society’s 79th Annual Forum and Technology Display, West Palm Beach, FL, 2023.
- [10] J. I. Pedrero, M. Pleguezuelos and M. Muñoz, “Contact stress calculation of undercut spur and helical gear teeth,” *Mechanism and Machine Theory*, vol. 46, no. 11, pp. 1633-1646, 2011.
- [11] T.D. Mathur, E.C. Smith, L. Chang and R.C. Bill, “Contact mechanics and elasto-hydrodynamic lubrication analysis of internal-external straight bevel gear mesh in a pericyclic drive,” in International Design Engineering Technical Conferences and Computers and Information in Engineering Conference, Cleveland, Ohio, USA, 2017.
- [12] F. OSWALD, H. LIN, C.H. Liou and M. VALCO, “Dynamic analysis of spur gears using computer program DANST,” in 29th Joint Propulsion Conference and Exhibit, 1993.
- [13] F.B. Oswald, H.H. Lin and I.R. Delgado, “NASA Technical Memorandum 107291 Technical Report ARL.TR.1189 -Dynamic Analysis of Spur Gear Transmissions (DANST) -PC Version 3.00 User Manual,” 1996.
- [14] A.H. Elkholy, A. Elsharkawy and A.S. Yigit, “Effect of Meshing Tooth Stiffness and Manufacturing Error on the Analysis of Straight Bevel Gears,” *Journal of Structural Mechanics*, vol. 26, no. 1, pp. 41-61, 1998.
- [15] R.G. Parker and J. Lin, “Mesh phasing relationships in planetary and epicyclic gears,” *Journal of Mechanical Design*, vol. 126, no. 2, pp. 365-370, 2004.
- [16] T.D. Mathur, E.C. Smith and R.C. Bill, “A Novel Loaded Tooth Contact Analysis Procedure With Application to Internal–External Straight Bevel Gear Mesh in a Pericyclic Drive,” *Journal of Tribology*, vol. 143, no. 10, 2021.

VERTIFLIGHT TECHNOLOGIES IN LEONARDO

Flight Condition Recognition, Simulation, System Design,
Tilt-Rotor technologies and System Integration

Editor in Chief

Vincenzo Sabbatino

Editorial office

Emidio Di Pietro
Giovanni Cocca
Marco Morini
Patrizia Pozzoni

Published and Printed by:

Leonardo S.p.A.
Innovation
Piazza Monte Grappa, 4
00195 Roma

The Editorial Team thanks Luca Medici
for serving as the Guest Editor, and Paolo Casanova and Danilo Defant for their contribution.

The POLARIS Innovation Journal is an editorial initiative of the unit Innovation.
Other initiatives of the POLARIS Innovation Journal are the Paperbacks and the Lunchtime Webinars.
The Journal invites questions and suggestions from readers.
Contact the Editorial Office at: polaris@leonardo.com

Scan this QR code to access the web version



https://www.leonardo.com/polaris_2023_49/

In compliance with the Leonardo sustainability policies,
and to contribute reducing the environmental footprint of the Company,
the POLARIS Innovation Journal is printed on certified paper (Xerox International Certificate).
The POLARIS Innovation Journal is published biannually.

Issue 49 – Oct 2023

VERTIFLIGHT TECHNOLOGIES IN LEONARDO

Flight Condition Recognition, Simulation, System Design,
Tilt-Rotor technologies and System Integration

PROPRIETARY NOTICE

Contents of the POLARIS Innovation Journal are the personal responsibility of the authors of the individual papers.

Authors are entirely responsible for opinions expressed in articles appearing in the Journal, and these opinions are not to be construed as official or reflecting the views of Leonardo or of the above-listed Committees and Offices.

Every article is certified by its corresponding author as being “Company General Use”

in compliance with the Security rules and regulations of the Company

The name POLARIS Innovation Journal is property of Leonardo. All rights reserved.

Copyright 2023 Leonardo S.p.A. Reproduction in whole or in part
is prohibited except by permission of the publisher.

